The Astrophysical Journal, 746:154 (22pp), 2012 February 20 doi:10.1088/0004-637X/746/2/154

A REVISED AGE FOR UPPER SCORPIUS AND THE STAR FORMATION HISTORY AMONG THE F-TYPE MEMBERS OF THE SCORPIUS–CENTAURUS OB ASSOCIATION

Mark J. Pecaut[1], Eric E. Mamajek[1,3], and Eric J. Bubar[1,2]
[1] Department of Physics and Astronomy, University of Rochester, Rochester, NY 14627-0171, USA
[2] Department of Biology and Physical Sciences, Marymount University, Arlington, VA 22207-4299, USA
Received 2011 August 8; accepted 2011 December 2; published 2012 February 2

ABSTRACT

We present an analysis of the ages and star formation history of the F-type stars in the Upper Scorpius (US), Upper Centaurus–Lupus (UCL), and Lower Centaurus–Crux (LCC) subgroups of Scorpius–Centaurus (Sco-Cen), the nearest OB association. Our parent sample is the kinematically selected *Hipparcos* sample of de Zeeuw et al., restricted to the 138 F-type members. We have obtained classification-resolution optical spectra and have also determined the spectroscopic accretion disk fraction. With *Hipparcos* and 2MASS photometry, we estimate the reddening and extinction for each star and place the candidate members on a theoretical H-R diagram. For each subgroup we construct empirical isochrones and compare to published evolutionary tracks. We find that (1) our empirical isochrones are consistent with the previously published age-rank of the Sco-Cen subgroups; (2) subgroups LCC and UCL appear to reach the main-sequence turn-on at spectral types ∼F4 and ∼F2, respectively. An analysis of the A-type stars shows US reaching the main sequence at about spectral type ∼A3. (3) The median ages for the pre-main-sequence members of UCL and LCC are 16 Myr and 17 Myr, respectively, in agreement with previous studies, however we find that (4) Upper Sco is much older than previously thought. The luminosities of the F-type stars in US are typically a factor of ∼2.5 less luminous than predicted for a 5 Myr old population for four sets of evolutionary tracks. We re-examine the evolutionary state and isochronal ages for the B-, A-, and G-type Upper Sco members, as well as the evolved M supergiant Antares, and estimate a revised mean age for Upper Sco of $11 \pm 1 \pm 2$ Myr (statistical, systematic). Using radial velocities and *Hipparcos* parallaxes we calculate a lower limit on the kinematic expansion age for Upper Sco of >10.5 Myr (99% confidence). However, the data are statistically consistent with no expansion. We reevaluate the inferred masses for the known substellar companions in Upper Sco using the revised age and find that the inferred masses are typically ∼20%–70% higher than the original estimates which had assumed a much younger age; specifically, we estimate the mass of 1RXS J1609-2105b to be 14^{+2}_{-3} $M_{\rm Jup}$, suggesting that it is a brown dwarf rather than a planet. Finally, we find the fraction of F-type stars exhibiting Hα emission and/or a *K*-band excess consistent with accretion to be 0/17 (<19%; 95% CL) in US at ∼11 Myr, while UCL has 1/41 (2^{+5}_{-1}%; 68% CL) accretors and LCC has 1/50 (2^{+4}_{-1}%; 68% CL) accretors at ∼16 Myr and ∼17 Myr, respectively.

Key words: circumstellar matter – Hertzsprung–Russell and C–M diagrams – open clusters and associations: individual (Scorpius–Centaurus) – stars: individual (Antares, 1RXS J160930.3-210459) – stars: pre-main sequence

1. INTRODUCTION AND BACKGROUND

Embedded clusters hosting massive stars dominate the star formation of the galaxy (Lada & Lada 2003), and OB associations appear to be the unbound "fossils" of dissolved embedded clusters. Subgroups within OB associations are thought to be an approximately "coeval" stellar population (e.g., Briceño et al. 2007), sharing a common age, chemical abundance, and velocity. Ages of stellar populations are a critical key to determining the evolutionary timescales of various stages of circumstellar disk evolution and, together with the accretion disk fraction, constrain planet formation timescales (e.g., Chen et al. 2011; Mamajek 2009). In addition, the estimated masses for very low mass companions to members of the stellar population depend critically on the assumed age (e.g., Lafrenière et al. 2008; Ireland et al. 2011). It is therefore important to estimate a consistent age for the stellar population so it can be used with confidence for such calculations, and to periodically test this derived age with constantly improving observational data against modern theoretical evolutionary models.

In this paper, we explore the F-type (∼1.2–1.7 $M_{\odot}$ for ages ∼10–15 Myr) stars of Scorpius–Centaurus (Sco-Cen), the nearest OB association (Preibisch & Mamajek 2008). Sco-Cen consists of three subgroups: Upper Scorpius (US), Upper Centaurus–Lupus (UCL), and Lower Centaurus–Crux (LCC), with mean distances of 145 pc, 140 pc, and 118 pc, respectively (de Zeeuw et al. 1999). As the nearest site of recent massive star formation, the stellar membership of Sco-Cen offers important samples of young stars for understanding circumstellar disk evolution across the mass spectrum.

Ages for the Sco-Cen subgroups have been determined primarily from the main-sequence turnoff and the low-mass pre-main-sequence (PMS) population combining H-R diagram positions with theoretical evolutionary tracks. For the high-mass stars, this has been performed most recently for UCL and LCC by Mamajek et al. (2002), obtaining ages ∼17 Myr and ∼16 Myr, respectively. The most recent published age-dating of the massive stars of US was performed by de Geus et al. (1989), obtaining an age of ∼5 Myr using the evolutionary tracks of Maeder (1981) and corroborated by Preibisch et al. (2002).

Our goal in this paper is to explore the star formation history and accretion disk fraction of the F-type members of three subgroups of Scorpius–Centaurus: US, UCL, and LCC.

[3] Current address: Cerro Tololo Inter-American Observatory, Casilla 603, La Serena, Chile.

Specifically, we have employed the kinematically selected *Hipparcos* sample from de Zeeuw et al. (1999) and have (1) placed them on a theoretical H-R diagram, (2) used published evolutionary tracks to obtain ages and masses, (3) compared the star formation history of the F-type stars with previous results (Mamajek et al. 2002; Preibisch et al. 2002), and (4) estimated the spectroscopic accretion disk fraction to constrain the disk dispersal timescale for intermediate-mass stars.

2. SAMPLE SELECTION

Our sample of Sco-Cen F-stars was taken from the kinematic analysis of de Zeeuw et al. (1999) which used both a refurbished convergent point method (de Bruijne 1999a) and the "spaghetti method" (Hoogerwerf & Aguilar 1999) to identify members based on *Hipparcos* positions, parallax, and proper motions. The kinematic selection methods are described in detail in de Zeeuw et al. (1999), but briefly, the selection applied the convergent point method and spaghetti method independently to early-type stars to create a list of "secure" members of the OB association. A kinematic solution is obtained using both methods and the results of this are applied to a broader collection of stars in the *Hipparcos* catalog, with appropriate position, proper motion, and distance limits for the particular OB association. Stars selected by both methods are included in their membership lists, and they also provide an estimate of the overall number of interlopers present in the membership list for each subgroup. For our sample (F-type candidate members only) the number of expected interlopers is ∼5 in US, ∼15 in UCL, and ∼9 in LCC. Further critical examination of the F-type samples was conducted by Chen et al. (2011).

3. OBSERVATIONS AND DATA

Low-resolution blue (∼3700 Å–5200 Å) and red (∼5600 Å–6900 Å) optical spectra were obtained from the SMARTS 1.5 m telescope at Cerro Tololo Inter-American Observatory (CTIO). Observations were made in queue mode with the RC spectrograph between 2009 February and 2009 December. The blue spectra were obtained with a 600 grooves mm^{-1} grating (designated 26/Ia) blazed at 4450 Å and no filter, while the red spectra were taken with an 831 grooves mm^{-1} grating (47/Ib) blazed at 7100 Å and GG495 filter. Both setups use a slit width of 110.5 μm. One comparison lamp of HeAr and neon for blue and red, respectively, was taken immediately before three consecutive exposures of each target. The blue spectra have a resolution of 4.3 Å or $R \sim 1100$ at Hβ and the red spectra have a resolution of 3.1 Å or $R \sim 2100$ at Hα.

The data were reduced using Fred Walter's SMARTS RC Spectrograph IDL pipeline.[4] The three object images are median combined, bias-trimmed, overscan- and bias-subtracted, then flat-fielded and wavelength-calibrated. Finally, we normalize the spectra to the continuum with a sixth-order spline in preparation for spectral classification.

We have adopted V magnitudes and $B-V$ and $V-I_C$ colors from the *Hipparcos* (Perryman & ESA 1997) catalog and JHK_S photometry from 2MASS (Skrutskie et al. 2006). We have taken proper motion data, used to calculate a kinematically improved parallax (more on this in Section 4.3) from both the revised *Hipparcos* data (van Leeuwen 2007) and the *Tycho-2* (Høg et al. 2000) catalogs. We used revised *Hipparcos* data if the fit obtained is that for a single star (i.e., a five-parameter solution with no peculiarities). Otherwise we use the long-baseline proper motions from the *Tycho-2* catalog. The motivation behind this choice is to use the most precise and accurate proper motion data to calculate the most accurate kinematic parallax possible. The presence of a companion or other peculiarities present in the astrometric solution could significantly influence the detected proper motions if a three-year baseline is used, as with the *Hipparcos* data, whereas the longer baseline proper motions from the *Tycho-2* catalog should be less affected. Our input data are listed in Table 1.

4. ANALYSIS

4.1. Spectral Classification

The optical spectra were visually classified using the primary temperature classification spectral features for F-type stars: the strength and profile of the Balmer lines, followed by several metal lines including the *G* band at ∼4310 Å (Gray & Corbally 2009). PMS stars may exhibit enhanced chromospheric activity, which will weaken the strength of the Balmer absorption lines or they may be seen in emission. In this case a correct classification can still be obtained using the wings of the hydrogen line profiles (R. O. Gray 2010, private communication). In addition to the hydrogen lines and the strength and shape of the *G* band, we used the strength of the temperature-sensitive Ca I λ4226 and Fe I λ4383 lines to confirm the classifications, although in this temperature region we found them less useful than the *G* band.

Stellar spectral classification is greatly facilitated by the ability to visually overlay the object on spectral standards obtained with the same spectral resolution. To that end, we developed a visual classification tool (*sptool*) which presents the object spectrum against two standard star spectra and allows the user to change the comparison standards with a single keystroke. The tool allows the classifier to easily move in temperature and luminosity subtype space by using the arrow keys on the keyboard. The tool, written in Python, is freely available online[5] and only requires a dense grid of spectral standard stars.

To obtain accurate spectral classifications for our program stars, we obtained a grid of optical spectra of F-type MK spectral standard stars with the same telescope and setup as our program stars. Our choices for standards are listed in Table 2. Although there are many choices for spectral standards, ours were chosen based on a careful consideration of the consistency of previous classifications and accessibility from the SMARTS 1.5 m telescope at CTIO.

Unfortunately, A8V and F4V spectral standards do not appear in the literature (e.g., Morgan & Keenan 1973; Gray & Corbally 2009), and the only A9V standard that we could find in the literature (44 Cet = HR 401; Gray & Garrison 1989) had several discrepant published spectral types. For subtypes A8V and A9V we adopted a star that had been assigned that spectral class by at least one expert classifier and had colors representative of other stars of the same classification. We adopted the Hyades member HD 27561 as an F4V standard. The star was originally classified as F4V by Morgan & Hiltner (1965), and its *Hipparcos* $B-V$ color (0.41) is intermediate in color between the F3V and F5V standards classified by Morgan (and retained as standards by Morgan & Abt 1973, Morgan et al. 1978, and Gray 1989)—HD 26015 (F3V standard, $B-V = 0.40$) and HD 27524 (F5V standard, $B-V = 0.434$)—both of which are

[4] http://www.astro.sunysb.edu/fwalter/SMARTS/smarts_15msched.html#RCpipeline

[5] http://www.pas.rochester.edu/∼mpecaut/sptool/

Table 1
Input Observables For Sco-Cen Candidate Members

HIP	Group	2MASS	$\mu_{\alpha*}$ (mas yr^{-1})	μ_{δ} (mas yr^{-1})	V (mag)	$B-V$ (mag)	J (mag)	H (mag)	K_S (mag)	PM References
55334	LCC	11195276-7037065	-43.28 ± 0.66	4.41 ± 0.58	8.14	0.413 ± 0.004	7.319 ± 0.024	7.153 ± 0.027	7.084 ± 0.021	H
56227	LCC	11313495-6743545	-41.49 ± 0.61	-3.09 ± 0.51	8.34	0.316 ± 0.017	7.779 ± 0.027	7.683 ± 0.036	7.612 ± 0.021	H
56673	LCC	11371464-6940272	-42.40 ± 1.30	-5.20 ± 1.30	6.62	0.518 ± 0.006	5.688 ± 0.024	5.459 ± 0.024	5.326 ± 0.023	T
57595	LCC	11482700-5409185	-27.60 ± 2.00	-4.50 ± 1.90	9.45	0.475 ± 0.024	8.512 ± 0.027	8.285 ± 0.047	8.215 ± 0.024	T
57950	LCC	11530799-5643381	-38.41 ± 0.71	-10.37 ± 0.58	8.26	0.401 ± 0.016	7.467 ± 0.024	7.312 ± 0.027	7.276 ± 0.027	H
58075	LCC	11543559-5443572	-29.38 ± 0.83	-7.05 ± 0.82	9.02	0.418 ± 0.019	8.228 ± 0.056	7.997 ± 0.047	7.925 ± 0.027	H
58146	LCC	11552884-6211471	-34.95 ± 0.46	-4.51 ± 0.39	7.86	0.391 ± 0.012	7.051 ± 0.020	6.914 ± 0.024	6.833 ± 0.027	H
58167	LCC	11554354-5410506	-36.17 ± 0.73	-8.56 ± 0.62	8.30	0.404 ± 0.013	7.473 ± 0.024	7.361 ± 0.051	7.284 ± 0.020	H
58220	LCC	11562655-5849168	-37.38 ± 0.74	-8.22 ± 0.58	8.48	0.443 ± 0.013	7.672 ± 0.021	7.490 ± 0.034	7.390 ± 0.023	H
58528	LCC	12000940-5707021	-38.71 ± 0.74	-9.28 ± 0.62	8.54	0.484 ± 0.018	7.707 ± 0.029	7.480 ± 0.047	7.423 ± 0.029	H
58899	LCC	12044446-5221156	-36.98 ± 0.74	-11.46 ± 0.70	8.41	0.416 ± 0.012	7.597 ± 0.018	7.421 ± 0.034	7.346 ± 0.033	H
59084	LCC	12070066-5941408	-29.18 ± 0.77	-13.38 ± 0.67	8.64	0.230 ± 0.015	7.932 ± 0.023	7.775 ± 0.026	7.710 ± 0.021	H
59481	LCC	12115882-5046124	-33.35 ± 0.71	-11.01 ± 0.70	8.48	0.426 ± 0.011	7.704 ± 0.030	7.564 ± 0.047	7.508 ± 0.021	H
59603	LCC	12132235-5653356	-33.18 ± 0.90	-7.01 ± 0.77	8.56	0.425 ± 0.014	7.699 ± 0.019	7.520 ± 0.033	7.433 ± 0.031	H
59693	LCC	12142864-4736461	-27.43 ± 0.98	-7.27 ± 0.75	9.70	0.542 ± 0.030	8.632 ± 0.024	8.360 ± 0.034	8.300 ± 0.023	H
59716	LCC	12145071-5547235	-37.40 ± 1.80	-10.70 ± 1.80	8.45	0.480 ± 0.014	7.516 ± 0.019	7.357 ± 0.034	7.280 ± 0.024	T
59764	LCC	12151855-6325301	-36.66 ± 0.79	-10.32 ± 0.66	8.43	0.605 ± 0.016	7.246 ± 0.026	6.960 ± 0.027	6.850 ± 0.021	H
59781	LCC	12152822-6232207	-20.00 ± 1.90	0.40 ± 1.60	8.84	0.573 ± 0.015	7.821 ± 0.030	7.538 ± 0.033	7.504 ± 0.027	T
59960	LCC	12175319-5558319	-38.79 ± 0.58	-12.21 ± 0.56	7.80	0.458 ± 0.003	6.946 ± 0.030	6.759 ± 0.038	6.683 ± 0.026	H
60205	LCC	12204420-5215249	-25.33 ± 1.37	-8.38 ± 1.30	10.06	0.521 ± 0.042	9.120 ± 0.023	8.868 ± 0.025	8.827 ± 0.022	H
60245	LCC	12211172-4803192	-27.94 ± 0.69	-8.54 ± 0.56	8.90	0.387 ± 0.014	8.165 ± 0.023	8.015 ± 0.038	8.003 ± 0.038	H
60348	LCC	12222484-5101343	-35.30 ± 1.20	-11.70 ± 1.10	8.80	0.490 ± 0.014	7.950 ± 0.023	7.759 ± 0.038	7.671 ± 0.021	T
60513	LCC	12241829-5858352	-28.77 ± 0.70	-12.50 ± 0.59	8.52	0.414 ± 0.014	7.687 ± 0.023	7.498 ± 0.047	7.457 ± 0.026	H
60567	LCC	12245491-5200157	-28.72 ± 1.43	-8.87 ± 1.06	9.77	0.541 ± 0.028	8.698 ± 0.029	8.469 ± 0.044	8.386 ± 0.033	H
61049	LCC	12304626-5811168	-38.21 ± 0.78	-12.72 ± 0.72	8.59	0.518 ± 0.013	7.465 ± 0.021	7.189 ± 0.024	7.072 ± 0.024	H
61086	LCC	12311262-5141497	-24.20 ± 2.40	2.60 ± 2.30	10.57	0.441 ± 0.069	9.836 ± 0.023	9.729 ± 0.025	9.653 ± 0.019	T
61087	LCC	12311264-6154315	-35.53 ± 0.66	-12.45 ± 0.54	8.00	0.504 ± 0.010	7.012 ± 0.021	6.819 ± 0.027	6.740 ± 0.024	H
62032	LCC	12425487-5049000	-26.30 ± 0.94	-8.01 ± 0.87	8.74	0.345 ± 0.016	8.054 ± 0.019	7.925 ± 0.051	7.896 ± 0.024	H
62056	LCC	12430803-5028125	-29.40 ± 1.88	-7.43 ± 1.39	10.48	0.523 ± 0.067	9.453 ± 0.023	9.205 ± 0.022	9.138 ± 0.019	H
62134	LCC	12440192-5330205	-30.30 ± 0.93	-9.96 ± 0.81	8.62	0.408 ± 0.015	7.879 ± 0.020	7.730 ± 0.027	7.708 ± 0.026	H
62171	LCC	12442659-5420480	-34.18 ± 0.97	-12.97 ± 0.83	8.90	0.445 ± 0.018	8.048 ± 0.027	7.828 ± 0.053	7.748 ± 0.024	H
62427	LCC	12473870-5824567	-29.97 ± 0.94	-8.15 ± 0.70	9.28	0.454 ± 0.023	8.363 ± 0.026	8.172 ± 0.036	8.122 ± 0.029	H
62428	LCC	12473920-5817511	-33.25 ± 0.42	-14.18 ± 0.33	6.95	0.261 ± 0.005	6.418 ± 0.021	6.376 ± 0.031	6.294 ± 0.020	H
62431	LCC	12474180-5825558	-30.20 ± 1.80	-4.30 ± 1.40	8.02	0.379 ± 0.009	7.250 ± 0.021	7.084 ± 0.038	6.987 ± 0.029	T
62657	LCC	12501971-4951488	-36.61 ± 0.86	-16.47 ± 0.59	8.91	0.502 ± 0.014	8.002 ± 0.023	7.830 ± 0.057	7.717 ± 0.024	H
62674	LCC	12503322-4730552	-26.31 ± 1.30	-11.52 ± 0.95	10.27	0.420 ± 0.020	9.460 ± 0.024	9.321 ± 0.023	9.294 ± 0.023	H
62677	LCC	12503583-6805288	-29.70 ± 1.90	-15.20 ± 1.90	9.36	0.535 ± 0.030	8.314 ± 0.019	8.155 ± 0.033	8.109 ± 0.025	T
63022	LCC	12545378-5102499	-29.78 ± 0.93	-10.69 ± 0.88	9.77	0.402 ± 0.029	9.050 ± 0.021	8.902 ± 0.022	8.852 ± 0.019	H
63041	LCC	12550391-6338267	-39.46 ± 0.60	-11.97 ± 0.57	8.05	0.383 ± 0.004	7.339 ± 0.032	7.210 ± 0.031	7.137 ± 0.031	H
63272	LCC	12575777-5236546	-34.24 ± 0.63	-13.67 ± 0.50	8.40	0.351 ± 0.011	7.684 ± 0.024	7.557 ± 0.049	7.456 ± 0.016	H
63435	LCC	12595641-5054350	-30.13 ± 0.88	-9.20 ± 0.74	9.21	0.489 ± 0.018	8.239 ± 0.023	8.001 ± 0.031	7.988 ± 0.033	H
63439	LCC	12595987-5023224	-28.60 ± 1.12	-12.37 ± 0.55	9.14	0.413 ± 0.018	8.278 ± 0.023	8.145 ± 0.051	8.039 ± 0.021	H
63527	LCC	13010436-5308084	-30.64 ± 0.51	-16.81 ± 0.41	7.79	0.358 ± 0.015	7.055 ± 0.018	6.938 ± 0.038	6.860 ± 0.017	H
63836	LCC	13045944-4723485	-31.16 ± 0.92	-17.66 ± 0.64	9.00	0.447 ± 0.023	8.090 ± 0.026	7.892 ± 0.036	7.868 ± 0.029	H
63886	LCC	13053261-5832078	-38.09 ± 0.76	-16.39 ± 0.63	8.15	0.404 ± 0.001	7.387 ± 0.023	7.297 ± 0.040	7.223 ± 0.027	H
63975	LCC	13063577-4602018	-33.50 ± 2.00	-18.30 ± 1.90	7.48	0.405 ± 0.021	6.725 ± 0.026	6.594 ± 0.027	6.489 ± 0.024	T
64044	LCC	13073350-5254198	-32.43 ± 0.96	-19.08 ± 0.69	8.83	0.540 ± 0.014	7.823 ± 0.029	7.614 ± 0.038	7.513 ± 0.021	H
64184	LCC	13091620-6018300	-40.04 ± 0.56	-19.31 ± 0.50	8.20	0.445 ± 0.015	7.403 ± 0.019	7.226 ± 0.023	7.163 ± 0.031	H
64316	LCC	13105627-5147063	-26.41 ± 1.32	-11.09 ± 1.39	10.19	0.493 ± 0.055	9.297 ± 0.027	9.072 ± 0.023	9.012 ± 0.021	H
64322	LCC	13105901-6205157	-26.86 ± 0.67	-12.75 ± 0.61	8.23	0.436 ± 0.015	7.419 ± 0.026	7.250 ± 0.049	7.194 ± 0.031	H
64877	LCC	13175541-6100388	-38.32 ± 0.69	-16.45 ± 0.69	8.47	0.456 ± 0.015	7.622 ± 0.032	7.411 ± 0.036	7.408 ± 0.031	H
64995	LCC	13191952-5928202	-33.53 ± 0.62	-17.81 ± 0.56	8.23	0.398 ± 0.015	7.504 ± 0.023	7.385 ± 0.036	7.337 ± 0.023	H
65136	LCC	13205161-4843196	-26.57 ± 0.78	-16.23 ± 0.68	9.23	0.391 ± 0.020	8.519 ± 0.030	8.421 ± 0.069	8.326 ± 0.024	H
65617	LCC	13271219-5938142	-27.73 ± 1.19	-13.03 ± 0.91	9.60	0.549 ± 0.019	8.642 ± 0.021	8.398 ± 0.026	8.360 ± 0.023	H
65875	LCC	13300897-5829043	-31.32 ± 0.80	-18.64 ± 0.63	8.08	0.498 ± 0.015	7.166 ± 0.023	6.973 ± 0.040	6.897 ± 0.029	H
66285	LCC	13350807-5821593	-33.80 ± 1.70	-13.40 ± 1.30	8.34	0.533 ± 0.003	7.316 ± 0.021	7.068 ± 0.036	7.036 ± 0.024	T
67068	LCC	13444395-4917577	-28.64 ± 0.83	-21.77 ± 0.65	8.45	0.401 ± 0.015	7.686 ± 0.029	7.520 ± 0.029	7.475 ± 0.029	H
67230	LCC	13463539-6204096	-29.97 ± 0.60	-20.59 ± 0.66	8.03	0.474 ± 0.007	7.136 ± 0.027	6.931 ± 0.027	6.888 ± 0.021	H
67428	LCC	13490922-5413422	-22.29 ± 1.06	-17.72 ± 0.91	8.91	0.520 ± 0.018	7.938 ± 0.024	7.713 ± 0.042	7.631 ± 0.023	H
67497	UCL	13495450-5014238	-29.34 ± 0.59	-20.63 ± 0.50	8.40	0.377 ± 0.012	7.708 ± 0.026	7.568 ± 0.049	7.516 ± 0.024	H
67957	UCL	13550129-5045020	-24.64 ± 1.11	-16.06 ± 0.82	9.23	0.592 ± 0.024	8.050 ± 0.020	7.763 ± 0.036	7.658 ± 0.033	H
67970	UCL	13550999-5044429	-27.18 ± 0.87	-19.51 ± 0.65	8.70	0.427 ± 0.018	7.874 ± 0.024	7.695 ± 0.046	7.676 ± 0.020	H
68335	UCL	13591805-5153342	-27.67 ± 0.60	-22.13 ± 0.51	8.43	0.489 ± 0.013	7.528 ± 0.029	7.325 ± 0.049	7.215 ± 0.026	H
68534	LCC	14014704-6118459	-12.20 ± 1.70	-20.00 ± 1.70	9.32	0.400 ± 0.495	8.421 ± 0.020	8.225 ± 0.024	8.168 ± 0.020	T
69291	UCL	14105961-3616016	-24.71 ± 0.87	-20.29 ± 0.77	8.61	0.411 ± 0.015	7.849 ± 0.026	7.729 ± 0.044	7.666 ± 0.018	H

Table 1
(Continued)

HIP	Group	2MASS	$\mu_{\alpha*}$ (mas yr^{-1})	μ_{δ} (mas yr^{-1})	V (mag)	$B-V$ (mag)	J (mag)	H (mag)	K_S (mag)	PM References
69327	UCL	14111998-5437560	-33.70 ± 0.79	-26.23 ± 0.61	8.54	0.348 ± 0.014	7.868 ± 0.021	7.746 ± 0.031	7.705 ± 0.020	H
69720	UCL	14161698-5349021	-27.15 ± 0.81	-17.69 ± 0.79	8.81	0.391 ± 0.017	8.048 ± 0.021	7.905 ± 0.034	7.856 ± 0.020	H
70350	UCL	14233787-4357426	-29.41 ± 0.75	-29.20 ± 0.72	8.13	0.569 ± 0.015	7.006 ± 0.023	6.723 ± 0.031	6.680 ± 0.021	H
70376	UCL	14235639-5029585	-28.10 ± 2.00	-18.10 ± 1.80	9.20	0.662 ± 0.031	8.041 ± 0.020	7.718 ± 0.026	7.661 ± 0.021	T
70558	UCL	14255851-4449232	-21.35 ± 1.10	-17.16 ± 0.89	9.06	0.394 ± 0.029	8.334 ± 0.029	8.155 ± 0.029	8.128 ± 0.027	H
70689	UCL	14273044-5231304	-30.80 ± 0.72	-24.32 ± 0.88	8.53	0.373 ± 0.015	7.802 ± 0.024	7.622 ± 0.059	7.510 ± 0.023	H
70833	UCL	14290715-4321427	-28.98 ± 0.94	-20.16 ± 1.04	8.82	0.423 ± 0.017	8.020 ± 0.023	7.841 ± 0.040	7.787 ± 0.020	H
71023	UCL	14313339-4445019	-22.50 ± 1.19	-17.76 ± 0.80	8.94	0.394 ± 0.019	8.185 ± 0.027	8.085 ± 0.046	7.974 ± 0.024	H
71767	UCL	14404593-4247063	-16.74 ± 1.08	-20.68 ± 1.32	9.02	0.496 ± 0.023	8.096 ± 0.023	7.834 ± 0.049	7.770 ± 0.023	H
72033	UCL	14440435-4059223	-20.25 ± 1.35	-21.30 ± 1.34	9.17	0.635 ± 0.035	8.024 ± 0.035	7.743 ± 0.036	7.578 ± 0.017	H
72099	UCL	14445687-3422537	-16.38 ± 1.97	-20.16 ± 1.68	9.66	0.540 ± 0.040	8.651 ± 0.018	8.426 ± 0.024	8.397 ± 0.025	H
72164	UCL	14453753-4001493	-18.10 ± 1.70	-13.40 ± 1.60	8.86	0.433 ± 0.107	8.222 ± 0.021	8.105 ± 0.059	7.986 ± 0.031	T
73666	UCL	15033194-3122343	-27.23 ± 0.80	-27.60 ± 0.63	7.94	0.534 ± 0.015	6.900 ± 0.021	6.724 ± 0.029	6.641 ± 0.029	H
73667	UCL	15033198-4035230	-20.80 ± 1.40	-12.60 ± 1.20	8.82	0.471 ± 0.018	7.919 ± 0.029	7.698 ± 0.034	7.673 ± 0.027	T
73742	UCL	15042588-4758374	-20.57 ± 0.79	-26.96 ± 0.78	8.61	0.589 ± 0.018	7.517 ± 0.020	7.263 ± 0.021	7.216 ± 0.017	H
73913	UCL	15061795-3524222	-19.63 ± 0.88	-19.83 ± 0.67	8.71	0.340 ± 0.015	8.003 ± 0.023	7.838 ± 0.040	7.826 ± 0.036	H
74499	UCL	15132796-3308502	-25.94 ± 1.06	-27.75 ± 0.87	8.77	0.461 ± 0.024	7.878 ± 0.023	7.732 ± 0.051	7.651 ± 0.024	H
74772	UCL	15165338-4934175	-13.70 ± 1.70	-18.91 ± 1.57	9.82	0.435 ± 0.048	8.894 ± 0.026	8.772 ± 0.024	8.687 ± 0.020	H
74865	UCL	15175611-3028414	-22.19 ± 1.34	-28.20 ± 0.98	8.89	0.511 ± 0.047	8.064 ± 0.020	7.901 ± 0.044	7.808 ± 0.021	H
74959	UCL	15190542-3621440	-24.59 ± 1.29	-25.59 ± 1.24	9.37	0.469 ± 0.026	8.393 ± 0.018	8.223 ± 0.033	8.154 ± 0.029	H
75367	UCL	15240425-4109416	-21.28 ± 1.50	-18.57 ± 1.18	10.26	0.427 ± 0.067	9.118 ± 0.021	8.888 ± 0.025	8.825 ± 0.019	H
75459	UCL	15245612-3730055	-15.10 ± 1.30	-35.20 ± 1.30	8.51	0.500 ± 0.495	7.692 ± 0.019	7.489 ± 0.033	7.450 ± 0.024	T
75480	UCL	15250939-2634310	-21.79 ± 0.99	-31.31 ± 0.80	8.33	0.404 ± 0.018	7.566 ± 0.024	7.433 ± 0.042	7.376 ± 0.026	H
75491	UCL	15251605-3809286	-20.12 ± 0.96	-23.34 ± 0.83	8.45	0.416 ± 0.017	7.622 ± 0.021	7.473 ± 0.057	7.431 ± 0.026	H
75683	UCL	15274232-3614131	-21.56 ± 2.34	-25.34 ± 1.91	9.47	0.473 ± 0.015	8.608 ± 0.030	8.414 ± 0.036	8.374 ± 0.024	H
75824	UCL	15292309-4009499	-19.37 ± 1.17	-17.33 ± 1.05	8.81	0.465 ± 0.017	7.958 ± 0.023	7.763 ± 0.033	7.770 ± 0.027	H
75891	UCL	15300427-4107101	-19.78 ± 1.03	-25.70 ± 0.97	8.62	0.437 ± 0.016	7.793 ± 0.024	7.608 ± 0.024	7.566 ± 0.021	H
75933	UCL	15303404-3829463	-22.77 ± 0.94	-19.28 ± 0.92	8.91	0.481 ± 0.015	7.959 ± 0.024	7.771 ± 0.047	7.719 ± 0.027	H
76084	UCL	15322013-3108337	-18.87 ± 0.98	-21.85 ± 0.89	8.62	0.446 ± 0.001	7.764 ± 0.026	7.562 ± 0.031	7.507 ± 0.027	H
76457	UCL	15365348-3810511	-25.70 ± 1.20	-33.90 ± 1.30	8.18	0.396 ± 0.015	7.454 ± 0.024	7.299 ± 0.023	7.234 ± 0.017	T
76501	UCL	15372791-3229060	-22.85 ± 1.27	-28.98 ± 1.10	8.62	0.501 ± 0.019	7.722 ± 0.024	7.570 ± 0.059	7.516 ± 0.023	H
76875	UCL	15415321-3453199	-21.26 ± 1.25	-27.76 ± 1.05	8.37	0.397 ± 0.006	7.606 ± 0.019	7.471 ± 0.038	7.410 ± 0.023	H
77038	UCL	15434763-3528298	-17.23 ± 1.60	-22.63 ± 1.27	9.15	0.478 ± 0.023	8.223 ± 0.024	8.028 ± 0.031	7.918 ± 0.029	H
77432	UCL	15482478-4237049	-16.36 ± 1.19	-30.31 ± 1.02	8.96	0.434 ± 0.020	8.112 ± 0.019	7.939 ± 0.051	7.872 ± 0.027	H
77502	UCL	15493198-3115396	-14.33 ± 1.09	-21.90 ± 0.94	8.89	0.444 ± 0.021	8.088 ± 0.029	7.927 ± 0.031	7.874 ± 0.029	H
77520	UCL	15493963-3846391	-16.02 ± 1.75	-25.33 ± 1.29	9.25	0.440 ± 0.015	8.324 ± 0.027	8.131 ± 0.034	7.996 ± 0.026	H
77713	UCL	15515975-3449414	-20.73 ± 1.32	-19.13 ± 1.38	9.15	0.450 ± 0.024	8.322 ± 0.024	8.160 ± 0.033	8.113 ± 0.021	H
77780	UCL	15525514-4548032	-27.80 ± 1.55	-29.64 ± 1.14	9.13	0.590 ± 0.020	8.176 ± 0.019	7.969 ± 0.024	7.914 ± 0.024	H
77813	US	15532089-1923535	-10.88 ± 1.56	-27.39 ± 1.22	9.25	0.739 ± 0.020	7.782 ± 0.026	7.418 ± 0.049	7.302 ± 0.024	H
78043	UCL	15560561-3653345	-18.60 ± 1.66	-24.26 ± 1.50	8.97	0.474 ± 0.020	8.153 ± 0.021	7.974 ± 0.042	7.940 ± 0.020	H
78233	US	15582930-2124039	-7.89 ± 1.51	-20.75 ± 1.17	9.06	0.513 ± 0.020	7.994 ± 0.021	7.811 ± 0.046	7.690 ± 0.033	H
78555	UCL	16021853-3516117	-15.50 ± 1.26	-30.86 ± 0.97	8.64	0.387 ± 0.018	7.926 ± 0.023	7.816 ± 0.047	7.734 ± 0.027	H
78663	US	16033342-3008133	-14.49 ± 1.18	-23.37 ± 1.05	8.91	0.496 ± 0.020	7.973 ± 0.026	7.784 ± 0.047	7.702 ± 0.024	H
78881	UCL	16060937-3802180	-14.90 ± 1.30	-26.30 ± 1.70	8.03	0.523 ± 0.015	7.083 ± 0.019	6.881 ± 0.034	6.790 ± 0.018	T
78977	US	16071778-2203364	-10.59 ± 1.34	-25.74 ± 1.00	8.70	0.654 ± 0.022	7.543 ± 0.027	7.146 ± 0.047	7.047 ± 0.031	H
79054	US	16081050-2351024	-12.67 ± 0.96	-19.71 ± 0.83	9.16	0.501 ± 0.026	8.149 ± 0.024	7.909 ± 0.040	7.828 ± 0.024	H
79083	US	16083514-2045296	-9.28 ± 1.61	-24.61 ± 1.04	8.41	0.605 ± 0.020	7.094 ± 0.030	6.773 ± 0.042	6.677 ± 0.026	H
79097	US	16084366-2522367	-13.28 ± 1.01	-22.78 ± 0.77	8.76	0.520 ± 0.019	7.601 ± 0.027	7.328 ± 0.042	7.254 ± 0.026	H
79258	US	16103595-3245427	-6.00 ± 1.20	-18.97 ± 1.02	9.32	0.475 ± 0.028	8.433 ± 0.026	8.228 ± 0.034	8.206 ± 0.034	H
79288	US	16105511-2531214	-11.44 ± 0.99	-25.71 ± 0.77	8.97	0.463 ± 0.020	8.081 ± 0.023	7.949 ± 0.031	7.882 ± 0.020	H
79369	US	16115551-2106179	-7.38 ± 1.73	-22.49 ± 1.29	8.97	0.489 ± 0.020	7.855 ± 0.021	7.652 ± 0.038	7.562 ± 0.026	H
79516	UCL	16133433-4549035	-20.06 ± 1.18	-28.84 ± 1.18	8.91	0.458 ± 0.019	8.021 ± 0.029	7.851 ± 0.046	7.792 ± 0.024	H
79606	US	16144016-2014030	-17.28 ± 1.49	-28.79 ± 1.12	9.14	0.755 ± 0.020	7.526 ± 0.029	7.235 ± 0.051	7.072 ± 0.023	H
79643	US	16150927-2345348	-8.27 ± 2.06	-23.27 ± 1.19	9.53	0.568 ± 0.015	8.363 ± 0.029	8.146 ± 0.049	8.028 ± 0.018	H
79644	US	16151045-2207099	-9.57 ± 1.96	-21.07 ± 1.44	10.20	0.742 ± 0.058	8.897 ± 0.021	8.658 ± 0.049	8.539 ± 0.025	H
79673	UCL	16153714-4138585	-20.46 ± 1.15	-28.03 ± 1.12	8.84	0.410 ± 0.015	8.047 ± 0.024	7.904 ± 0.024	7.839 ± 0.033	H
79710	UCL	16160384-4904293	-19.85 ± 1.16	-30.60 ± 0.83	8.42	0.358 ± 0.017	7.774 ± 0.021	7.648 ± 0.029	7.605 ± 0.026	H
79742	UCL	16162838-3844123	-17.12 ± 1.73	-30.21 ± 1.52	9.16	0.492 ± 0.028	8.275 ± 0.018	8.061 ± 0.038	8.065 ± 0.016	H
79908	UCL	16183856-3839117	-25.21 ± 1.61	-34.60 ± 1.29	9.05	0.601 ± 0.021	8.010 ± 0.020	7.769 ± 0.047	7.689 ± 0.024	H
79910	US	16183914-2135341	-10.91 ± 1.46	-25.94 ± 1.30	9.00	0.569 ± 0.020	7.838 ± 0.021	7.612 ± 0.031	7.542 ± 0.023	H
79977	US	16192923-2124132	-10.93 ± 1.09	-26.24 ± 0.98	9.09	0.492 ± 0.020	8.062 ± 0.019	7.854 ± 0.031	7.800 ± 0.024	H
80586	US	16271252-2711219	-14.00 ± 1.50	-22.80 ± 1.40	8.20	0.473 ± 0.001	7.419 ± 0.019	7.270 ± 0.046	7.193 ± 0.026	T
80663	UCL	16280830-4654043	-9.49 ± 2.57	-20.12 ± 2.20	10.20	0.519 ± 0.043	9.028 ± 0.021	8.813 ± 0.023	8.742 ± 0.021	H
80896	US	16311105-2959523	-15.26 ± 1.49	-25.40 ± 0.92	8.53	0.433 ± 0.015	7.693 ± 0.019	7.548 ± 0.063	7.452 ± 0.021	H
80921	UCL	16312848-4455439	-11.12 ± 2.15	-20.32 ± 1.88	10.31	0.475 ± 0.062	9.039 ± 0.021	8.819 ± 0.024	8.761 ± 0.025	H

Table 1
(Continued)

HIP	Group	2MASS	$\mu_{\alpha*}$ (mas yr^{-1})	μ_{δ} (mas yr^{-1})	V (mag)	$B-V$ (mag)	J (mag)	H (mag)	K_S (mag)	PM References
81455	US	16381081-2940401	-7.04 ± 1.62	-25.64 ± 1.15	9.15	0.465 ± 0.020	8.256 ± 0.021	8.046 ± 0.034	8.036 ± 0.018	H
81851	US	16430538-2627307	-12.88 ± 1.34	-33.34 ± 0.95	8.44	0.406 ± 0.015	7.693 ± 0.027	7.566 ± 0.044	7.508 ± 0.021	H
82218	US	16474733-1952319	-15.01 ± 1.26	-26.27 ± 0.87	9.05	0.485 ± 0.020	8.057 ± 0.027	7.887 ± 0.036	7.800 ± 0.029	H
82319	US	16491221-2242416	-6.40 ± 1.40	-22.60 ± 1.40	8.89	0.427 ± 0.028	8.050 ± 0.024	7.900 ± 0.031	7.883 ± 0.036	T
82534	US	16521331-2655108	-13.09 ± 1.02	-29.15 ± 0.73	8.30	0.386 ± 0.018	7.600 ± 0.026	7.430 ± 0.040	7.370 ± 0.033	H
82569	UCL	16524171-3845372	-8.30 ± 1.06	-23.00 ± 0.82	8.85	0.461 ± 0.015	7.913 ± 0.029	7.727 ± 0.047	7.558 ± 0.023	H
82747	UCL	16544485-3653185	-8.91 ± 2.11	-29.61 ± 1.51	9.21	0.746 ± 0.040	7.676 ± 0.026	7.059 ± 0.033	6.503 ± 0.020	H
83159	UCL	16594248-3726168	-8.31 ± 1.40	-29.11 ± 1.01	9.02	0.395 ± 0.032	8.148 ± 0.026	7.961 ± 0.031	7.916 ± 0.017	H

Note. Proper motion references: H: van Leeuwen (2007); T: Høg et al. (2000).

Table 2
Spectral Standard Stars Used for Classification

Standard	Spectral Type	$B-V$ (mag)	Instrument/Source	References
HD 158352	A8 V	0.237	SMARTS 1.5 m/Rochester	1, A
HD 73450	A9 V	0.251	SMARTS 1.5 m/Rochester	2, B
HD 23585	F0 V	0.291	SMARTS 1.5 m/NStars	3, C
HD 27397	F0 IV	0.283	SMARTS 1.5 m/Stony Brook	3, A
HD 89025	F0 IIIa	0.307	SMARTS 1.5 m/Rochester	3, A
HD 167858	F1 V	0.312	SMARTS 1.5 m/Rochester	4, A
HD 113139	F2 V	0.368	DSO/NStars	3, A
HD 40535	F2 III-IV	0.333	SMARTS 1.5 m/Stony Brook	4, A
HD 26015	F3 V	0.397	SMARTS 1.5 m/Stony Brook	3, A
HD 27561	F4 V	0.412	SMARTS 1.5 m/Rochester	5, A
HD 27524	F5 V	0.434	SMARTS 1.5 m/Rochester	3, A
HD 17918	F5 III	0.457	SMARTS 1.5 m/Stony Brook	7, A
HD 30652	F6 IV-V	0.484	SMARTS 1.5 m/Stony Brook	3, A
HD 160365	F6 III-IV	0.567	SMARTS 1.5 m/Nstars	3, A
HD 222368	F7 V	0.507	SMARTS 1.5 m/Stony Brook	3, A
HD 27808	F8 V	0.518	SMARTS 1.5 m/Stony Brook	3, A
HD 220657	F8 III	0.617	SMARTS 1.5 m/Stony Brook	3, A
HD 10647	F9 V	0.551	SMARTS 1.5 m/Stony Brook	6, A
HD 109358	G0 V	0.588	DSO/Nstars	3, A
HD 6903	G0 IIIa	0.697	SMARTS 1.5 m/Stony Brook	3, A

Notes. Spectral type sources: (1) Cowley et al. 1969; (2) Gray & Corbally 2002; (3) Gray et al. 2001; (4) Gray & Garrison 1989; (5) Morgan & Hiltner 1965; (6) Gray et al. 2006; (7) Gray 1989; $B-V$ color sources: (A) van Leeuwen 2007; (B) Neckel & Klare 1980; (C) Mermilliod 2006.

also Hyads. We have confirmed that its spectrum is intermediate between the F3V and F5V standards. For the A8V standard, we adopt the star HD 158352 (HR 6507), which was classified as A8V by Cowley et al. (1969), Abt & Morrell (1995), and as A8Vp by Mora et al. (2001). For the A9V standard, we adopted the Praesepe member HD 73450 (BS Cnc), based on its A9V classifications by Bidelman (1956), Abt (1986), and Gray & Corbally (2002). We verified that the adopted A8V and A9V "standards" had optical spectra that were morphologically intermediate between the A7V and F0V MK standards.

With our visual classification tool and a complete grid of dwarfs, we iteratively classified the 138 program stars at least four times before settling on a final spectral type. We conservatively estimate our classifications to be correct to within one subtype.

Spectral types for many of our candidate members are available through the Michigan Spectral Survey (Houk & Smith-Moore 1988; Houk 1982, 1978; Houk & Cowley 1975) which allows us to directly compare our newly obtained spectral types

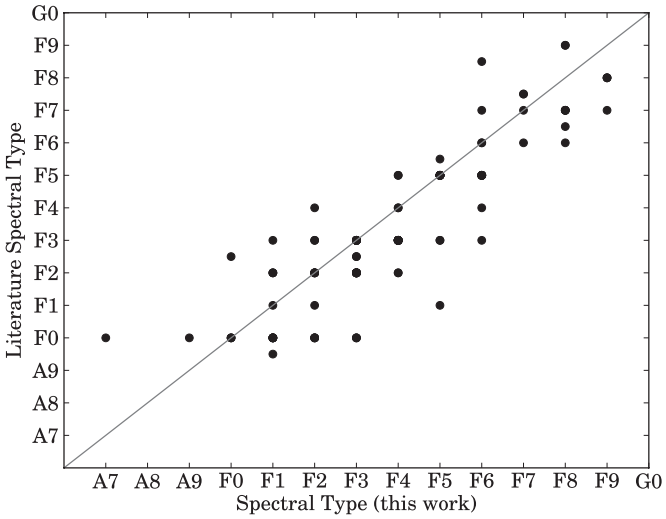

Figure 1. Comparison of our newly obtained spectral types with those available in the literature: Houk & Smith-Moore (1988), Houk (1982, 1978), and Houk & Cowley (1975). A line with unit slope is plotted to guide the eye.

with past results from plate surveys. As Figure 1 shows, the newly obtained spectral types agree quite well with those obtained in the Michigan Spectral Survey. The average difference is small: 0.5 ± 1.1 (1σ). The Houk classifications are based on comparison to the "MK" standards from Johnson & Morgan (1953), whereas we have relied heavily on the "revised MK" F-type standards from Morgan et al. (1978, "MK78") (these later types have been adopted by Gray, Garrison, Corbally, and collaborators in their surveys). Any systematic differences in the classifications likely come from differences in the choice of standard star, which differs between us and Houk mostly among the earliest and latest F stars.

4.2. Extinction

To calculate individual extinctions in the Johnson–Cousins and 2MASS bands, we constructed a modern spectral type-intrinsic color calibration with $B-V$, $V-I_c$, $V-K_S$, $J-H$, and $H-K_S$ colors using samples of nearby dwarf stars from the *Hipparcos* catalog (Perryman & ESA 1997), normal cool dwarfs from Neill Reid's compiled photometric catalog for stars in the 3rd Catalog of Nearby Stars,[6] and a cross-matched catalog combining the new Gliese-2MASS catalog (Stauffer et al. 2010) and the catalog of average Johnson *UBV* photometry from Mermilliod (2006). For the *Hipparcos* sample, only dwarfs with

[6] http://www.stsci.edu/~inr/cmd.html

Table 3
Intrinsic Colors of Dwarfs and Adopted $T_{\rm eff}$, and BC Values

Spectral Type	$U-B$ (mag)	$B-V$ (mag)	$V-I_C$ (mag)	$V-J$ (mag)	$V-H$ (mag)	$V-K_S$ (mag)	BC_V (mag)	$T_{\rm eff}$ (K)
A0V	−0.014	0.000	0.004	0.046	0.014	0.042	−0.17	9550
A1V	0.033	0.043	0.044	0.094	0.070	0.101	−0.11	9200
A2V	0.063	0.074	0.092	0.167	0.158	0.192	−0.05	8760
A3V	0.077	0.090	0.110	0.197	0.196	0.231	−0.02	8550
A4V	0.097	0.140	0.165	0.296	0.318	0.355	0.00	8270
A5V	0.100	0.160	0.187	0.334	0.366	0.404	0.01	8080
A6V	0.098	0.170	0.198	0.355	0.391	0.429	0.02	8000
A7V	0.091	0.210	0.242	0.433	0.488	0.528	0.04	7800
A8V	0.082	0.253	0.291	0.512	0.589	0.632	0.04	7500
A9V	0.080	0.255	0.294	0.517	0.595	0.638	0.04	7440
F0V	0.053	0.294	0.339	0.589	0.687	0.732	0.03	7200
F1V	0.013	0.343	0.396	0.678	0.802	0.850	0.03	7030
F2V	−0.008	0.374	0.432	0.735	0.875	0.925	0.01	6810
F3V	−0.016	0.389	0.449	0.763	0.910	0.961	0.01	6720
F4V	−0.026	0.412	0.476	0.806	0.965	1.017	0.00	6640
F5V	−0.029	0.438	0.506	0.852	1.025	1.079	0.00	6510
F6V	−0.021	0.484	0.553	0.929	1.128	1.185	−0.01	6340
F7V	−0.012	0.510	0.579	0.971	1.184	1.244	−0.02	6240
F8V	0.000	0.530	0.599	1.004	1.229	1.290	−0.03	6150
F9V	0.014	0.552	0.620	1.040	1.277	1.340	−0.04	6040
G0V	0.049	0.588	0.656	1.097	1.355	1.421	−0.05	5940
G1V	0.067	0.604	0.672	1.123	1.390	1.458	−0.06	5880
G2V	0.120	0.642	0.706	1.185	1.473	1.545	−0.07	5780
G3V	0.152	0.661	0.722	1.217	1.516	1.590	−0.08	5700
G4V	0.175	0.674	0.733	1.239	1.546	1.621	−0.10	5640
G5V	0.185	0.680	0.738	1.249	1.559	1.635	−0.10	5620
G6V	0.229	0.704	0.759	1.290	1.614	1.693	−0.11	5580
G7V	0.243	0.713	0.766	1.303	1.632	1.712	−0.12	5520
G8V	0.284	0.737	0.786	1.344	1.686	1.768	−0.13	5490
G9V	0.358	0.777	0.820	1.409	1.774	1.861	−0.17	5340

luminosity class "V" and M_V within 1 mag of the Wright (2005) main sequence were selected, and only stars with parallaxes greater than 13.33 mas and relative parallax error less than 12.5% were included ($d < 75$ pc), to select those stars ostensibly within the "Local Bubble" which has negligible reddening. An intrinsic color sequence was constructed for B- through M-type stars, and the adopted intrinsic colors for a given dwarf spectral subtype were adopted based on a best $B-V$ color.[7] Our adopted intrinsic colors are in Table 3.

Many of the stars in our sample had very low extinction, and where we obtained a non-physical negative extinction we set the extinction to zero. We used a total-to-selective extinction of $R_V = 3.1$ and calculated A_V using the color excesses $E(B-V)$, $E(V-I_c)$, $E(V-J)$, $E(V-H)$, and $E(V-K_S)$ with the extinction ratios $A_{I_c}/A_V = 0.58$, $A_J/A_V = 0.27$, $A_H/A_V = 0.17$, $A_{K_S}/A_V = 0.11$ (Fiorucci & Munari 2003) to estimate extinctions for each star. We adopted the median A_V with the standard deviation as a conservative estimate of the uncertainty. These are listed in Table 4 with our other derived stellar parameters.

4.3. Distances

While the stars in our sample have been selected from the *Hipparcos* catalog and therefore have trigonometric parallaxes, we can refine the distance determination by employing moving cluster or "convergent point" parallaxes. This works by leveraging the longer-baseline astrometric measurements employed to determine proper motions and taking advantage of the common space motion for the group. Kinematically improved parallaxes have been shown to reduce scatter in the H-R diagram (see the Hyades in de Bruijne et al. 2001 for a good example) and a comparison with trigonometric parallaxes can further help identify interlopers. One caveat is that kinematic parallaxes are meaningless for stars which are not true members.

For our kinematic parallax calculations we followed Mamajek (2005) and used updated space motions for US, UCL, and LCC tabulated in Chen et al. (2011).[8] As described previously, we use proper motion data from the revised *Hipparcos* reduction (van Leeuwen 2007) for stars with single star (five-parameter) solutions and data from *Tycho-2* (Høg et al. 2000) otherwise. Our kinematic parallaxes compare very well with the *Hipparcos* trigonometric parallax data (Figure 2).

4.4. Field Star Contamination

While the techniques used to define the sample in de Zeeuw et al. (1999) ensure that the candidate members are physically coincident with Sco-Cen and moving with similar space motion, the selection is purely based on astrometric information. Here we attempt to use our spectroscopic observations in conjunction with an additional kinematic criterion to identify interlopers.

While the strength of Li can be used as a youth indicator in G- and K-type stars, older F-type stars will show less Li depletion and thus we cannot rely on this spectral feature alone

[7] Detailed notes for each subtype are available in the files listed at http://www.pas.rochester.edu/~emamajek/spt/ or http://www.ctio.noao.edu/~emamajek/spt/.

[8] These updated space motions should yield the best available predicted radial velocities and kinematic parallaxes.

Table 4
Stellar Parameters for F-type Sco-Cen Members

HIP	Group	Spectral Type	$\pi_{\rm kin}$ (mas)	EW(Hα) (Å)	A_V (mag)	$\log(T_{\rm eff})$ (dex)	$\log(L/L_\odot)$ (dex)	Mass D08 ($M_\odot$)	Age D08 (Myr)	Mass YY04 ($M_\odot$)	Age YY04 (Myr)	Mass S00 ($M_\odot$)	Age S00 (Myr)	Mass DM97 ($M_\odot$)	Age DM97 (Myr)	Median Mass ($M_\odot$)
55334	LCC	F2V	12.63 ± 0.90	4.7	0.12 ± 0.01	3.833 ± 0.006	0.49 ± 0.06	1.5[a]	>19	1.5[a]	>22	1.6[a]	...	1.5[a]	>25	1.5
56673	LCC	F5IVe	11.95 ± 0.90	−1.9	0.20 ± 0.05	3.814 ± 0.011	1.18 ± 0.07	2.0	5	2.0	5	2.0	7	2.0	5	2.0
57950	LCC	F3V	10.79 ± 0.73	4.9	0.04 ± 0.01	3.827 ± 0.005	0.55 ± 0.06	1.4	23	1.4	27	1.6[a]	>20	1.5[a]	>14	1.5
58075	LCC	F2V	8.13 ± 0.57	5.1	0.14 ± 0.04	3.833 ± 0.006	0.53 ± 0.06	1.5[a]	>14	1.5[a]	>15	1.6[a]	>30	1.5[a]	>17	1.5
58146	LCC	F3V	9.67 ± 0.65	5.1	0.04 ± 0.02	3.827 ± 0.005	0.80 ± 0.06	1.5	13	1.6	13	1.6	13	1.6	10	1.6
58167	LCC	F2V	9.96 ± 0.67	5.2	0.09 ± 0.02	3.833 ± 0.006	0.62 ± 0.06	1.5	19	1.5	21	1.6[a]	>16	1.5	22	1.5
58220	LCC	F4V	10.39 ± 0.71	4.3	0.08 ± 0.04	3.822 ± 0.009	0.51 ± 0.06	1.4	23	1.4	28	1.5[a]	>22	1.5[a]	>15	1.5
58528	LCC	F5V	10.68 ± 0.72	4.3	0.04 ± 0.06	3.814 ± 0.011	0.44 ± 0.06	1.4	21	1.4	26	1.5[a]	>23	1.4[a]	>15	1.4
58899	LCC	F3V	10.12 ± 0.66	5.1	0.08 ± 0.02	3.827 ± 0.005	0.56 ± 0.06	1.4	21	1.4	24	1.6[a]	>19	1.5[a]	>13	1.5
59084	LCC	F1V	8.38 ± 0.58	5.4	0.04 ± 0.20	3.845 ± 0.012	0.61 ± 0.10	1.6[a]	>12	1.6[a]	>14	1.6[a]	>14	1.6[a]	>12	1.6
59481	LCC	F3V	8.99 ± 0.58	4.9	0.02 ± 0.05	3.827 ± 0.005	0.61 ± 0.06	1.5	15	1.5	18	1.5	40	1.5	18	1.5
59603	LCC	F4V	8.86 ± 0.60	3.9	0.08 ± 0.03	3.822 ± 0.009	0.61 ± 0.06	1.4	16	1.5	17	1.5	24	1.5	16	1.5
59693	LCC	F7IV	7.07 ± 0.49	3.9	0.13 ± 0.04	3.795 ± 0.007	0.38 ± 0.06	1.2	20	1.3	19	1.3	40	1.3	18	1.3
59716	LCC	F5V	10.11 ± 0.79	4.5	0.11 ± 0.02	3.814 ± 0.011	0.55 ± 0.07	1.3	17	1.4	18	1.4	27	1.4	16	1.4
59764	LCC	F8V	10.11 ± 0.68	3.0	0.25 ± 0.05	3.788 ± 0.007	0.63 ± 0.06	1.4	12	1.5	11	1.4	15	1.4	12	1.4
59960	LCC	F5V	10.52 ± 0.67	4.4	0.04 ± 0.02	3.814 ± 0.011	0.75 ± 0.06	1.5	13	1.6	12	1.5	14	1.5	12	1.5
60205	LCC	F7V	6.76 ± 0.54	3.9	0.01 ± 0.03	3.795 ± 0.007	0.23 ± 0.07	1.2	32	1.2	83	1.4[a]	>62	1.3[a]	>19	1.3
60245	LCC	F1V	7.23 ± 0.46	5.2	0.10 ± 0.03	3.845 ± 0.012	0.66 ± 0.06	1.5	23	1.5	29	1.6[a]	>18	1.6[a]	>13	1.5
60348	LCC	F5V	9.34 ± 0.64	4.3	0.06 ± 0.06	3.814 ± 0.011	0.46 ± 0.07	1.4	18	1.4	22	1.5[a]	>20	1.4[a]	>15	1.4
60513	LCC	F4V	8.05 ± 0.53	5.0	0.04 ± 0.02	3.822 ± 0.009	0.70 ± 0.06	1.4	15	1.6	14	1.5	15	1.5	13	1.5
60567	LCC	F8V	7.54 ± 0.58	3.5	0.09 ± 0.03	3.788 ± 0.007	0.28 ± 0.07	1.2	23	1.2	22	1.4[a]	>22	1.2	22	1.2
61049	LCC	F8V	10.28 ± 0.66	3.6	0.17 ± 0.12	3.788 ± 0.007	0.52 ± 0.07	1.3	15	1.4	15	1.4	18	1.3	15	1.3
61087	LCC	F6V	9.72 ± 0.63	4.1	0.06 ± 0.01	3.802 ± 0.007	0.75 ± 0.06	1.5	11	1.6	11	1.5	14	1.6	9	1.5
62032	LCC	A9V	6.62 ± 0.45	6.7	0.25 ± 0.02	3.872 ± 0.017	0.85 ± 0.06	1.6	15	1.7	16	1.7	20	1.6	13	1.6
62134	LCC	F2V	7.79 ± 0.51	6.0	0.02 ± 0.05	3.833 ± 0.006	0.68 ± 0.06	1.5	14	1.6	15	1.5	23	1.5	14	1.5
62171	LCC	F3V	8.99 ± 0.58	5.1	0.17 ± 0.03	3.827 ± 0.005	0.50 ± 0.06	1.4	30	1.5[a]	>15	1.6[a]	>30	1.5[a]	>17	1.5
62427	LCC	F5V	7.70 ± 0.52	4.8	0.09 ± 0.03	3.814 ± 0.011	0.45 ± 0.06	1.4	18	1.4	25	1.5[a]	>23	1.4[a]	>15	1.4
62431	LCC	F1V	7.42 ± 0.64	6.1	0.13 ± 0.04	3.845 ± 0.012	1.00 ± 0.08	1.6	10	1.7	9	1.7	10	1.7	9	1.7
62657	LCC	F5V	9.59 ± 0.59	4.3	0.13 ± 0.05	3.814 ± 0.011	0.42 ± 0.06	1.3	26	1.3	33	1.5[a]	>30	1.4[a]	>16	1.4
62677	LCC	F5IV-V	8.39 ± 0.72	4.3	0.25 ± 0.04	3.814 ± 0.011	0.41 ± 0.08	1.3	29	1.3	43	1.5[a]	>25	1.4[a]	>15	1.4
63041	LCC	F1V	10.38 ± 0.65	5.8	0.07 ± 0.04	3.845 ± 0.012	0.67 ± 0.06	1.5	21	1.5	24	1.6[a]	>16	1.5	23	1.5
63272	LCC	F1V	8.80 ± 0.53	5.6	0.05 ± 0.03	3.845 ± 0.012	0.67 ± 0.05	1.5	21	1.5	25	1.6[a]	>17	1.5	25	1.5
63435	LCC	F6V	7.35 ± 0.47	4.5	0.04 ± 0.03	3.802 ± 0.007	0.50 ± 0.06	1.3	18	1.4	17	1.4	19	1.3	16	1.3
63439	LCC	F4V	7.35 ± 0.49	4.9	0.04 ± 0.04	3.822 ± 0.009	0.53 ± 0.06	1.4	20	1.4	23	1.5[a]	>19	1.5[a]	>14	1.5
63527	LCC	F1V	8.34 ± 0.49	5.4	0.06 ± 0.02	3.845 ± 0.012	0.96 ± 0.05	1.6	10	1.7	10	1.7	11	1.7	9	1.7
63836	LCC	F6V	8.30 ± 0.50	4.4	0.00 ± 0.03	3.802 ± 0.007	0.47 ± 0.05	1.3	19	1.4	18	1.4	28	1.3	17	1.3
63886	LCC	F3V	10.09 ± 0.62	5.1	0.00 ± 0.05	3.827 ± 0.005	0.63 ± 0.06	1.5	15	1.5	15	1.5	25	1.5	17	1.5
63975	LCC	F2V	8.77 ± 0.67	5.1	0.07 ± 0.03	3.833 ± 0.006	1.05 ± 0.07	1.7	8	1.8	8	1.7	9	1.8	8	1.8
64044	LCC	F6IV	8.89 ± 0.55	3.1	0.14 ± 0.03	3.802 ± 0.007	0.53 ± 0.06	1.3	17	1.4	17	1.4	18	1.4	16	1.4
64184	LCC	F4V	10.84 ± 0.65	5.0	0.02 ± 0.04	3.822 ± 0.009	0.56 ± 0.06	1.4	16	1.4	19	1.5[a]	>16	1.4	27	1.4
64322	LCC	F2V	7.29 ± 0.46	4.7	0.13 ± 0.03	3.833 ± 0.006	0.93 ± 0.06	1.6	10	1.7	10	1.7	11	1.7	9	1.7
64877	LCC	F4V	10.10 ± 0.61	4.8	0.11 ± 0.04	3.822 ± 0.009	0.55 ± 0.06	1.4	17	1.4	20	1.5[a]	>17	1.5[a]	>13	1.5
64995	LCC	F3V	9.11 ± 0.55	5.5	0.00 ± 0.05	3.827 ± 0.005	0.69 ± 0.06	1.5	14	1.6	14	1.5	17	1.5	13	1.5

Table 4
(Continued)

HIP	Group	Spectral Type	$\pi_{\rm kin}$ (mas)	EW(Hα) (Å)	A_V (mag)	$\log(T_{\rm eff})$ (dex)	$\log(L/L_\odot)$ (dex)	Mass D08 ($M_\odot$)	Age D08 (Myr)	Mass YY04 ($M_\odot$)	Age YY04 (Myr)	Mass S00 ($M_\odot$)	Age S00 (Myr)	Mass DM97 ($M_\odot$)	Age DM97 (Myr)	Median Mass ($M_\odot$)
65136	LCC	F0V	7.12 ± 0.43	6.2	0.19 ± 0.06	3.855 ± 0.010	0.57 ± 0.06	1.6[a]	>24	1.6[a]	...	1.7[a]	...	1.6[a]	...	1.6
65617	LCC	F6V	7.29 ± 0.50	3.6	0.09 ± 0.06	3.802 ± 0.007	0.37 ± 0.07	1.3	22	1.3	21	1.5[a]	>19	1.3	27	1.3
65875	LCC	F6V	8.60 ± 0.52	4.1	0.00 ± 0.03	3.802 ± 0.007	0.80 ± 0.05	1.6	10	1.6	10	1.5	12	1.6	9	1.6
67068	LCC	F3V	8.03 ± 0.46	4.7	0.02 ± 0.02	3.827 ± 0.005	0.72 ± 0.05	1.4	14	1.6	14	1.6	15	1.5	13	1.5
67230	LCC	F5V	8.55 ± 0.51	4.4	0.09 ± 0.02	3.814 ± 0.011	0.86 ± 0.05	1.6	11	1.6	11	1.6	12	1.6	9	1.6
67428	LCC	F6IV	6.44 ± 0.42	4.1	0.09 ± 0.02	3.802 ± 0.007	0.76 ± 0.06	1.5	11	1.6	11	1.5	13	1.6	9	1.5
67497	UCL	F2V	9.28 ± 0.65	5.3	0.00 ± 0.03	3.833 ± 0.006	0.61 ± 0.06	1.5	20	1.5	23	1.6[a]	>16	1.4	37	1.5
67957	UCL	F9V	7.57 ± 0.58	3.6	0.19 ± 0.06	3.781 ± 0.007	0.54 ± 0.07	1.4	13	1.5	12	1.4	17	1.4	13	1.4
67970	UCL	F3V	8.62 ± 0.62	4.2	0.10 ± 0.02	3.827 ± 0.005	0.59 ± 0.06	1.5	16	1.5	19	1.6[a]	>15	1.4	24	1.5
68335	UCL	F5V	9.13 ± 0.64	3.1	0.13 ± 0.03	3.814 ± 0.011	0.66 ± 0.06	1.4	15	1.5	13	1.5	15	1.5	13	1.5
68534	LCC	F2V	4.89 ± 0.52	5.0	0.23 ± 0.37	3.833 ± 0.006	0.88 ± 0.17	1.6	11	1.6	11	1.6	12	1.6	9	1.6
69291	UCL	F3V	7.58 ± 0.51	5.7	0.00 ± 0.05	3.827 ± 0.005	0.70 ± 0.06	1.5	14	1.6	14	1.6	16	1.5	13	1.5
69720	UCL	F3V	8.27 ± 0.59	5.0	0.00 ± 0.01	3.827 ± 0.005	0.54 ± 0.06	1.4	24	1.4	28	1.6[a]	>20	1.5[a]	>14	1.5
70350	UCL	F8V	10.02 ± 0.66	3.2	0.16 ± 0.04	3.788 ± 0.007	0.72 ± 0.06	1.6	10	1.6	10	1.5	13	1.6	9	1.6
70376	UCL	F9V	8.28 ± 0.73	3.1	0.24 ± 0.06	3.781 ± 0.007	0.50 ± 0.08	1.3	14	1.4	14	1.3	18	1.3	14	1.3
70558	UCL	F1V	6.63 ± 0.49	5.9	0.12 ± 0.04	3.845 ± 0.012	0.68 ± 0.07	1.5	20	1.5	22	1.6[a]	>14	1.5	21	1.5
70689	UCL	F2V	9.85 ± 0.68	5.2	0.02 ± 0.04	3.833 ± 0.006	0.51 ± 0.06	1.5[a]	>17	1.5[a]	>18	1.6[a]	...	1.5[a]	>18	1.5
71023	UCL	F2V	6.90 ± 0.51	5.5	0.05 ± 0.03	3.833 ± 0.006	0.67 ± 0.07	1.5	14	1.6	15	1.5	25	1.5	17	1.5
71767	UCL	F4V	6.28 ± 0.49	4.5	0.26 ± 0.04	3.822 ± 0.009	0.80 ± 0.07	1.5	12	1.6	12	1.6	13	1.6	10	1.6
72033	UCL	F7V	6.92 ± 0.53	2.7	0.29 ± 0.06	3.795 ± 0.007	0.68 ± 0.07	1.5	12	1.5	11	1.5	14	1.4	12	1.5
72099	UCL	F6V	5.98 ± 0.55	4.0	0.13 ± 0.03	3.802 ± 0.007	0.54 ± 0.08	1.3	17	1.4	17	1.4	18	1.4	15	1.4
72164	UCL	F2IV	5.22 ± 0.51	5.5	0.00 ± 0.12	3.833 ± 0.006	0.92 ± 0.10	1.6	11	1.6	10	1.7	11	1.7	9	1.7
73666	UCL	F3IV	8.84 ± 0.56	5.5	0.38 ± 0.03	3.827 ± 0.005	0.98 ± 0.06	1.7	9	1.7	9	1.7	10	1.7	8	1.7
73667	UCL	F4V	5.43 ± 0.47	4.8	0.15 ± 0.02	3.822 ± 0.009	0.96 ± 0.08	1.7	9	1.7	9	1.7	10	1.7	8	1.7
73742	UCL	F9V	8.04 ± 0.54	3.5	0.08 ± 0.02	3.781 ± 0.007	0.70 ± 0.06	1.6	9	1.6	10	1.5	13	1.6	9	1.6
73913	UCL	F1V	6.40 ± 0.43	5.8	0.04 ± 0.03	3.845 ± 0.012	0.82 ± 0.06	1.6	12	1.6	14	1.6	14	1.6	12	1.6
74499	UCL	F4V	8.66 ± 0.57	4.5	0.12 ± 0.02	3.822 ± 0.009	0.56 ± 0.06	1.4	16	1.5	19	1.5[a]	>16	1.4	25	1.4
74772	UCL	F3V	5.53 ± 0.52	4.6	0.17 ± 0.04	3.827 ± 0.005	0.55 ± 0.08	1.4	22	1.4	25	1.6[a]	>15	1.5[a]	>13	1.5
74865	UCL	F4V	8.16 ± 0.55	4.4	0.07 ± 0.12	3.822 ± 0.009	0.55 ± 0.08	1.4	17	1.4	20	1.5[a]	>15	1.4	39	1.4
74959	UCL	F6V	8.11 ± 0.57	3.9	0.02 ± 0.04	3.802 ± 0.007	0.35 ± 0.06	1.3	23	1.3	24	1.5[a]	>26	1.3	39	1.3
75367	UCL	F9V	6.44 ± 0.51	3.5	0.11 ± 0.23	3.781 ± 0.007	0.24 ± 0.12	1.1	24	1.2	23	1.4[a]	>19	1.2	22	1.2
75459	UCL	F3V	8.43 ± 0.60	4.8	0.11 ± 0.11	3.827 ± 0.005	0.69 ± 0.08	1.5	14	1.6	14	1.5	17	1.5	13	1.5
75480	UCL	F2V	8.65 ± 0.55	5.4	0.04 ± 0.03	3.833 ± 0.006	0.71 ± 0.06	1.5	14	1.6	14	1.6	18	1.5	13	1.5
75491	UCL	F2V	7.07 ± 0.47	4.3	0.12 ± 0.01	3.833 ± 0.006	0.87 ± 0.06	1.5	12	1.6	12	1.6	12	1.6	9	1.6
75683	UCL	F6V	7.60 ± 0.66	4.5	0.00 ± 0.03	3.802 ± 0.007	0.35 ± 0.08	1.3	23	1.3	23	1.5[a]	>19	1.3	35	1.3
75891	UCL	F3V	7.47 ± 0.51	5.4	0.12 ± 0.02	3.827 ± 0.005	0.75 ± 0.06	1.5	13	1.6	13	1.6	14	1.5	12	1.5
75933	UCL	F3V	6.71 ± 0.46	4.7	0.26 ± 0.02	3.827 ± 0.005	0.79 ± 0.06	1.5	13	1.6	13	1.6	13	1.5	12	1.5
76084	UCL	F1V	6.56 ± 0.45	5.4	0.30 ± 0.03	3.845 ± 0.012	0.93 ± 0.06	1.6	11	1.7	11	1.7	11	1.7	9	1.7
76457	UCL	F3V	9.73 ± 0.65	5.3	0.00 ± 0.03	3.827 ± 0.005	0.65 ± 0.06	1.5	15	1.5	15	1.5	22	1.5	14	1.5
76501	UCL	F3V	8.39 ± 0.57	5.0	0.19 ± 0.08	3.827 ± 0.005	0.68 ± 0.07	1.5	14	1.6	14	1.5	18	1.5	13	1.5
76875	UCL	F2V	7.96 ± 0.54	5.1	0.04 ± 0.02	3.833 ± 0.006	0.77 ± 0.06	1.5	13	1.6	14	1.6	14	1.5	13	1.6
77038	UCL	F5V	6.48 ± 0.50	4.7	0.12 ± 0.03	3.814 ± 0.011	0.66 ± 0.07	1.4	15	1.5	13	1.5	15	1.5	13	1.5
77432	UCL	F5V	7.84 ± 0.54	4.7	0.00 ± 0.01	3.814 ± 0.011	0.53 ± 0.06	1.3	17	1.4	19	1.4	37	1.4	16	1.4
77502	UCL	F4V	5.94 ± 0.42	4.7	0.00 ± 0.05	3.822 ± 0.009	0.80 ± 0.06	1.5	13	1.6	12	1.6	13	1.6	10	1.6

Table 4
(Continued)

HIP	Group	Spectral Type	π_{kin} (mas)	EW(Hα) (Å)	A_V (mag)	log(T_{eff}) (dex)	log($L/L_\odot$) (dex)	Mass D08 ($M_\odot$)	Age D08 (Myr)	Mass YY04 ($M_\odot$)	Age YY04 (Myr)	Mass S00 ($M_\odot$)	Age S00 (Myr)	Mass DM97 ($M_\odot$)	Age DM97 (Myr)	Median Mass ($M_\odot$)
77520	UCL	F4V	6.83 ± 0.53	4.8	0.16 ± 0.07	3.822 ± 0.009	0.60 ± 0.07	1.4	16	1.5	17	1.5	28	1.5	16	1.5
77713	UCL	F4V	6.28 ± 0.49	5.2	0.03 ± 0.04	3.822 ± 0.009	0.66 ± 0.07	1.4	15	1.5	14	1.5	17	1.5	13	1.5
77780	UCL	F7V	9.33 ± 0.65	3.9	0.00 ± 0.12	3.795 ± 0.007	0.32 ± 0.08	1.2	22	1.3	23	1.4[a]	>20	1.3	23	1.3
77813	US	F9V	7.97 ± 0.70	3.1	0.59 ± 0.10	3.781 ± 0.007	0.65 ± 0.09	1.5	10	1.5	10	1.4	14	1.5	11	1.5
78043	UCL	F4V	6.95 ± 0.55	5.1	0.04 ± 0.08	3.822 ± 0.009	0.64 ± 0.08	1.4	15	1.5	14	1.5	20	1.5	14	1.5
78233	US	F0IV	5.96 ± 0.56	6.2	0.67 ± 0.04	3.855 ± 0.010	0.99 ± 0.08	1.6	10	1.7	10	1.8	10	1.7	9	1.7
78555	UCL	F1V	7.78 ± 0.52	5.3	0.06 ± 0.04	3.845 ± 0.012	0.68 ± 0.06	1.5	20	1.5	22	1.6[a]	>14	1.5	20	1.5
78663	US	F6V	7.11 ± 0.59	4.6	0.03 ± 0.02	3.802 ± 0.007	0.65 ± 0.07	1.4	14	1.5	12	1.5	15	1.4	14	1.4
78881	UCL	F4V	6.86 ± 0.55	3.9	0.25 ± 0.05	3.822 ± 0.009	1.12 ± 0.07	1.9	7	1.9	7	1.8	8	1.9	7	1.9
78977	US	F8V	7.53 ± 0.64	3.1	0.38 ± 0.08	3.788 ± 0.007	0.83 ± 0.08	1.7	8	1.7	8	1.6	11	1.6	8	1.7
79054	US	F3V	6.24 ± 0.53	5.4	0.35 ± 0.05	3.827 ± 0.005	0.78 ± 0.08	1.5	13	1.6	13	1.6	13	1.5	12	1.5
79083	US	F3V	7.16 ± 0.63	4.2	0.76 ± 0.13	3.827 ± 0.005	1.13 ± 0.09	1.9	7	1.9	7	1.9	8	1.9	7	1.9
79097	US	F4V	6.99 ± 0.57	4.4	0.48 ± 0.12	3.822 ± 0.009	0.90 ± 0.09	1.6	11	1.6	10	1.6	11	1.7	9	1.6
79288	US	F2V	7.50 ± 0.60	5.1	0.21 ± 0.04	3.833 ± 0.006	0.65 ± 0.07	1.5	15	1.5	16	1.5	36	1.5	18	1.5
79369	US	F1V	6.42 ± 0.62	6.2	0.60 ± 0.10	3.845 ± 0.012	0.93 ± 0.09	1.6	11	1.7	11	1.7	11	1.7	9	1.7
79516	UCL	F5V	8.07 ± 0.56	4.0	0.05 ± 0.01	3.814 ± 0.011	0.54 ± 0.06	1.3	17	1.4	18	1.4	29	1.4	16	1.4
79606	US	F8V	9.19 ± 0.79	3.8	0.81 ± 0.14	3.788 ± 0.007	0.65 ± 0.09	1.5	11	1.5	11	1.4	15	1.4	12	1.5
79643	US	F3V	6.63 ± 0.62	4.8	0.56 ± 0.05	3.827 ± 0.005	0.67 ± 0.08	1.5	14	1.5	14	1.5	20	1.5	14	1.5
79644	US	F6V	6.30 ± 0.64	4.1	0.53 ± 0.11	3.802 ± 0.007	0.44 ± 0.10	1.3	20	1.3	19	1.3	39	1.3	18	1.3
79673	UCL	F4V	7.90 ± 0.54	4.3	0.00 ± 0.02	3.822 ± 0.009	0.57 ± 0.06	1.4	16	1.5	19	1.5[a]	>15	1.4	23	1.4
79710	UCL	F1V	8.45 ± 0.56	5.8	0.00 ± 0.05	3.845 ± 0.012	0.67 ± 0.06	1.5	21	1.5	24	1.6[a]	>15	1.5	23	1.5
79742	UCL	F6V	7.89 ± 0.59	4.5	0.00 ± 0.05	3.802 ± 0.007	0.45 ± 0.07	1.3	19	1.3	19	1.3	36	1.3	18	1.3
79908	UCL	F8V	9.71 ± 0.67	3.0	0.08 ± 0.07	3.788 ± 0.007	0.35 ± 0.07	1.2	21	1.2	20	1.3	30	1.2	19	1.2
79910	US	F4V	7.70 ± 0.69	4.2	0.49 ± 0.04	3.822 ± 0.009	0.72 ± 0.08	1.4	14	1.6	13	1.6	14	1.5	13	1.5
79977	US	F3V	7.79 ± 0.66	4.6	0.36 ± 0.05	3.827 ± 0.005	0.63 ± 0.08	1.5	15	1.5	15	1.5	27	1.5	17	1.5
80586	US	F5IV-V	7.02 ± 0.65	4.7	0.00 ± 0.10	3.814 ± 0.011	0.93 ± 0.09	1.6	9	1.7	9	1.6	11	1.7	8	1.7
80663	UCL	F1V	5.09 ± 0.61	5.4	0.68 ± 0.09	3.845 ± 0.012	0.67 ± 0.11	1.5	21	1.5	24	1.6[a]	>11	1.5	23	1.5
80896	US	F3V	7.67 ± 0.64	5.3	0.12 ± 0.02	3.827 ± 0.005	0.77 ± 0.07	1.5	13	1.6	13	1.6	13	1.5	12	1.5
80921	UCL	F2IV	5.30 ± 0.55	5.1	0.70 ± 0.21	3.833 ± 0.006	0.61 ± 0.12	1.5	20	1.5	23	1.6[a]	>12	1.4	30	1.5
81455	US	F5IV-V	7.01 ± 0.61	4.0	0.08 ± 0.02	3.814 ± 0.011	0.58 ± 0.08	1.3	17	1.4	17	1.5	21	1.4	15	1.4
81851	US	F3V	9.61 ± 0.78	5.2	0.00 ± 0.04	3.827 ± 0.005	0.56 ± 0.07	1.4	21	1.4	24	1.7[b]	>16	1.6[b]	>13	1.5
82218	US	F3V	8.39 ± 0.72	4.8	0.30 ± 0.02	3.827 ± 0.005	0.55 ± 0.08	1.4	22	1.4	25	1.7[b]	>16	1.6[b]	>13	1.5
82319	US	F3V	4.67 ± 0.96	5.5	0.10 ± 0.02	3.827 ± 0.005	1.05 ± 0.18	1.7	8	1.8	8	1.7	9	1.8	8	1.7
82534	US	F3V	8.55 ± 0.68	5.6	0.00 ± 0.03	3.827 ± 0.005	0.72 ± 0.07	1.4	14	1.6	14	1.6	15	1.5	13	1.5
82569	UCL	F4V	5.52 ± 0.38	4.0	0.18 ± 0.06	3.822 ± 0.009	0.95 ± 0.07	1.6	10	1.7	9	1.7	11	1.7	8	1.7
82747	UCL	F5Ve	6.94 ± 0.55	−0.7	0.96 ± 0.40	3.814 ± 0.011	0.92 ± 0.18	1.6	10	1.7	9	1.6	11	1.7	9	1.6
83159	UCL	F6V	6.79 ± 0.47	4.4	0.00 ± 0.08	3.802 ± 0.007	0.63 ± 0.07	1.4	14	1.5	12	1.4	16	1.4	14	1.4

Notes. Spectral types are from this work (Section 4.1). Uncertainties in log(T_{eff}) are calculated with a spectral type uncertainty of 1 subtype. In cases where the H-R diagram position was too close to the main sequence to yield a unique age, we provide upper limits (denoted by <) based on the 2σ upper limit on the luminosity. We have provided the median mass of all evolutionary tracks as the preferred mass for each member. Given the sizes of the observational uncertainties, it is preferable to adopt the median subgroup ages rather than these individual isochronal ages.

[a] Mass was derived assuming a 15 Myr age.

[b] Mass was derived assuming a 10 Myr age.

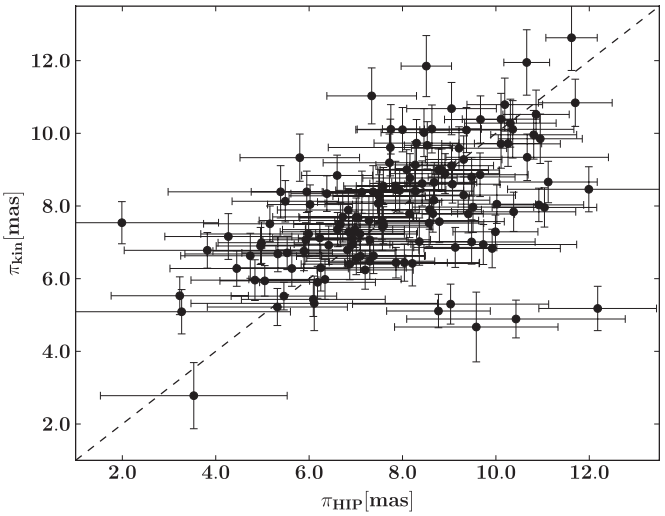

Figure 2. Comparison between *Hipparcos* trigonometric parallaxes and our kinematic parallaxes. A line with unit slope is plotted for comparison.

as a youth indicator in our sample (Balachandran 1991, however see Chen et al. 2011). We can, however, use Li to determine membership for any G/K stars which are companions to F-type stars, excluding or confirming the *pair* as members. Since our sample should consist of stars with predominantly dwarf and subgiant like gravities, we can also identify and exclude any giants found in our sample.

For members, the kinematic parallaxes should be in agreement with the trigonometric parallaxes. As a conservative criterion, we reject any star as a member if the difference between trigonometric parallax and kinematic parallax exceeds three times the uncertainty in those quantities added in quadrature. The motivation is that if the disagreement between the trigonometric and kinematic parallaxes is significant at the 3σ level, the object clearly has a different space motion than the group and can be safely rejected.

4.4.1. US Interlopers

Using our conservative kinematic rejection criteria, we rule out HIP 79258 as a member. A kinematic parallax of 5.11 ± 0.46 mas disagreed with the trigonometric parallax of 8.77 ± 1.11 mas at a confidence level $>3\sigma$. This is the only interloper we were able to identify in Upper Sco. We then expect that the US sample of 21 still contains ∼4 interlopers, ∼19%.

4.4.2. UCL Interlopers

Chen et al. (2011) reject HIP 70833 as a member of UCL since the cooler K3IV companion has an EW(Li λ6707) of only 0.01 Å. Chen et al. (2011) also reject HIP 75824 based on its low Li, with EW(Li λ6707) < 8 Å. Finally, HIP 69327 lies far below the zero-age main sequence, an unphysical portion of the H-R diagram, when the kinematic distance is used. As this is inconsistent with group membership, we identify it as an interloper.

With these non-members identified in UCL, there still remain ∼12 interlopers in our UCL sample of 53, or ∼23%.

4.4.3. LCC Interlopers

We reject one giant as an LCC member (HIP 62428, A7III; also rejected by Chen et al. 2011). It was also classified as a giant by Houk & Cowley (1975). Chen et al. (2011) also exclude HIP 66285 as a member, based on the lack of Li in its cooler comoving companion. HIP 59781 has a kinematic parallax of 5.18 ± 0.61 mas and a trigonometric parallax of 12.58 ± 1.26 mas, disagreeing above our 3σ threshold so we reject it. HIP 56227 has a kinematic parallax of 11.85 ± 0.84 mas and a trigonometric parallax of 8.51 ± 0.54 mas, also disagreeing above our 3σ threshold so we reject it. HIP 57595 has a trigonometric parallax of 3.53 ± 2.00 mas, which places it 165 pc from the mean distance of LCC. The *Tycho-2* proper motion for this star supports it being an unrelated background star—the kinematic parallax assuming it were a member of LCC places it even further from LCC ($\pi_{\rm kin} = 2.78 \pm 0.91$ mas), so we reject it. Finally, HIP 63022, HIP 61086, HIP 64316, HIP 62674, and HIP 62056 occupy an unphysical portion of the H-R diagram (below the zero-age main sequence) when the kinematic distances are used. As this is inconsistent with group membership, we identify these objects as interlopers.

With these interlopers identified in LCC, we believe that few, if any, of the remaining F-type stars are interlopers. Stars rejected as Sco-Cen members are listed in Table 5.

Table 5
Stars Rejected as Sco-Cen Members

Name	Spectral Type	Rejection Criteria	References
HIP 56227	F0IV	Kinematic parallax	1
HIP 57595	F6V	Trigonometric parallax	1
HIP 59781	F8V	Kinematic parallax	1
HIP 61086	F1V	HRD position	1
HIP 62056	F6V	HRD position	1
HIP 62428	A7III	Giant	1
HIP 62674	F3V	HRD position	1
HIP 63022	F0V	HRD position	1
HIP 64316	F3V	HRD position	1
HIP 66285	F7V	Companion Li-poor	1
HIP 69327	F1V	Kinematic parallax	1
HIP 70833	F3V	Companion Li-poor	1
HIP 75824	F3V	Li-poor	1
HIP 77457	A7IV	Kinematic parallax	2
HIP 79258	F4V	Kinematic parallax	1
HIP 81392	G2/3 V	Li-poor	2
HIP 83542	G8/K0 III	Giant	3

Notes. Spectral-type references: (1) this work; (2) Houk 1982; (3) Houk & Smith-Moore 1988.

4.5. Accretion Disk Fraction

We can examine our red optical spectra for evidence of accretion with the Hα feature. Accreting stars are thought to produce Hα emission due to hot infalling gas. For our accretion criterion we use the Hα full width at 10% peak (W_{10}(Hα)). White & Basri (2003) find that independent of spectral type, a full width at 10% peak >270 km s^{-1} is a good indicator of accretion. We do not estimate the mass accretion rates as that is beyond the scope of this study.

Using this criterion, we find only two stars in our sample with Hα emission consistent with accretion, both of which are binaries: the near-equal mass system AK Sco (HIP 82747; Andersen et al. 1989; Alencar et al. 2003) and the recently studied HD 101088 (HIP 56673; Bitner et al. 2010) with 10% peak widths of 710 km s^{-1} and 400 km s^{-1}, respectively. The spectral resolution of our red optical spectra at Hα is ∼140 km s^{-1}. The Hα profiles of these accretors are shown in Figure 3 along with the Hα profile of a non-accreting star in

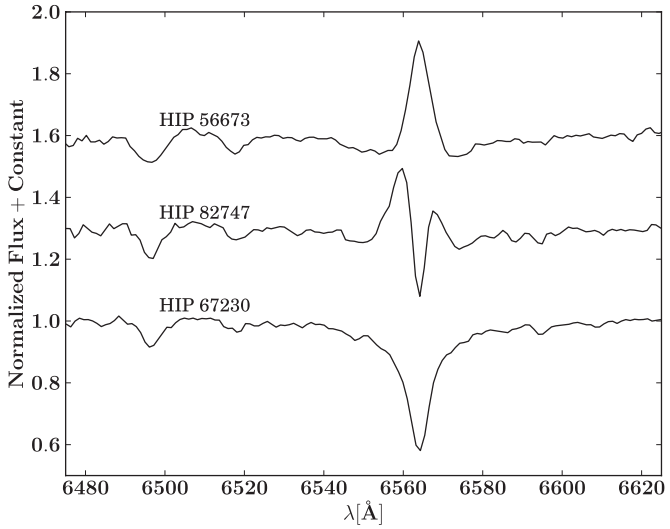

Figure 3. Hα region showing the two accretors in our sample, HD 101088 (HIP 56673, F5IVe) and AK Sco (HIP 82747, F5Ve), along with a non-accreting star (HIP 67230, F5V) of the same spectral type.

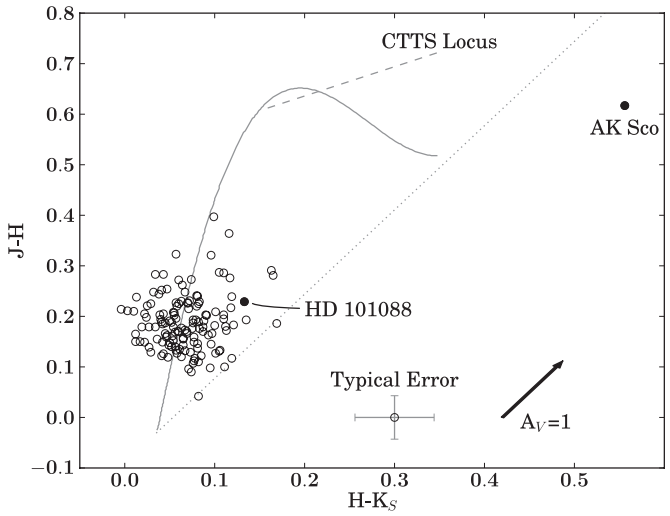

Figure 4. $H - K_S$ vs. $J - H$ for the program stars (not de-reddened; excluding interlopers). The solid line is the dwarf color locus and the dashed line is the classical T Tauri locus of Meyer et al. (1997) shown for reference. The dotted line is the reddening line of a standard A0 star. The solid circle outlier to the right is the eclipsing binary AK Sco, indicating that AK Sco's NIR color excess cannot be due to reddening.

our sample (HIP 67230, F5V) with the same spectral type as HD 101088 and AK Sco.

Using the classical T Tauri star color–color locus as determined by Meyer et al. (1997) and the intrinsic color locus of main-sequence stars we look for near-IR photometric signatures of accretion among our Sco-Cen members using 2MASS near-IR photometry. The plot in Figure 4 shows our Sco-Cen members (without reddening corrections applied) clustered around the locus with spread consistent with the uncertainties in the colors. The one obvious outlier with $H - K_S > 0.4$ is the known near-equal mass binary AK Sco referred to above. AK Sco is the star to the right of the locus, and its position is similar to that of the Herbig Ae/Be stars in Hernández et al. (2005).

Here we estimate the optical spectroscopic accretion disk fraction for F stars in our sample as 0/17 (<19%; 95% CL) for US, while UCL has 1/41 (2^{+5}_{-1}%; 68% CL) accretors and LCC has 1/50 (2^{+4}_{-1}%; 68% CL) F-type accretors. This compares

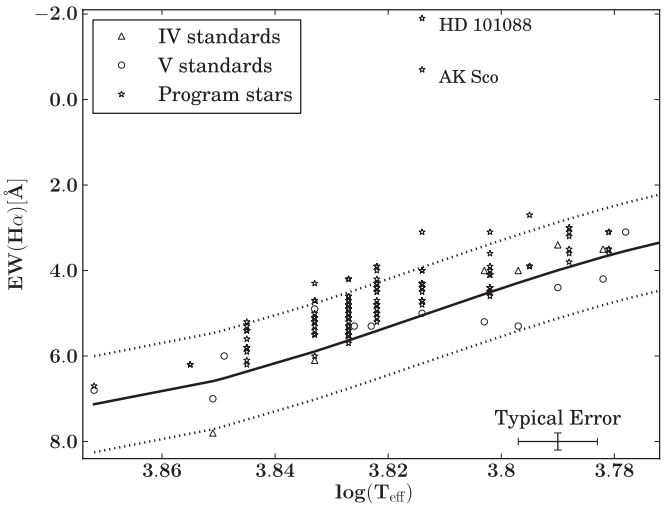

Figure 5. Hα EWs for the member stars compared with inactive field dwarfs and subgiants. The solid line is a third-order polynomial fit to the field stars and the dotted lines represent the 2σ scatter in the fit to the field stars. While the Sco-Cen program stars (interlopers not shown) are heavily represented above the trend line, most of them still lie within the 2σ spread of the field stars.

well with the Carpenter et al. (2006) *Spitzer* results in which 0/30 (<11%; 95% CL) F- and G-type stars were found to be accretors. The F-type results in UCL and LCC are consistent with the lower-mass G- and K-type stars studied by Mamajek et al. (2002), in which 1/110 ($0.9^{+2.0}_{-0.3}$%; 68% CL) members exhibited spectroscopic evidence of accretion.

As mentioned previously, PMS stars may exhibit enhanced chromospheric activity, which will manifest itself through partially filled Hα absorption lines. To examine this effect we measured the strength of the Hα lines with IRAF[9] for all our program stars as well as our spectral standards and plot the EW(Hα) against $T_{\rm eff}$ (Figure 5). The members plotted here indicate slightly enhanced chromospheric activity, although most are still within the 2σ spread of the spectral standards.

4.6. H-R Diagram

In order to compare Sco-Cen members with theoretical models and explore the star formation history of the F-type members, we construct a theoretical H-R diagram. The adopted effective temperature ($T_{\rm eff}$) scale and bolometric correction (BC) scale were taken from an extensive set of notes for spectral subtypes by EM.[6] This new $T_{\rm eff}$ scale comes from careful review and inter-comparison of spectroscopic and photometric temperature estimates for high quality MK standards as well as large samples of field dwarfs with MK classifications. The bolometric corrections are consensus estimates for the adopted temperatures, which rely heavily on the BCs for hot dwarf stars from Bessell et al. (1998) and for cool dwarf stars on the series of papers by Casagrande et al. (2006, 2008, 2010) (however BCs were also calculated interpolating the scales of Code et al. 1976, Balona 1994, Flower 1996, and Bertone et al. 2004 for comparison). Our temperatures and bolometric corrections are listed in Table 3.

We combine our extinction estimates with our kinematic parallaxes and *V*-band photometry (Perryman & ESA 1997) to estimate bolometric luminosity and place the members on a

[9] IRAF is distributed by the National Optical Astronomy Observatory, which is operated by the Association of Universities for Research in Astronomy, Inc., under cooperative agreement with the National Science Foundation.

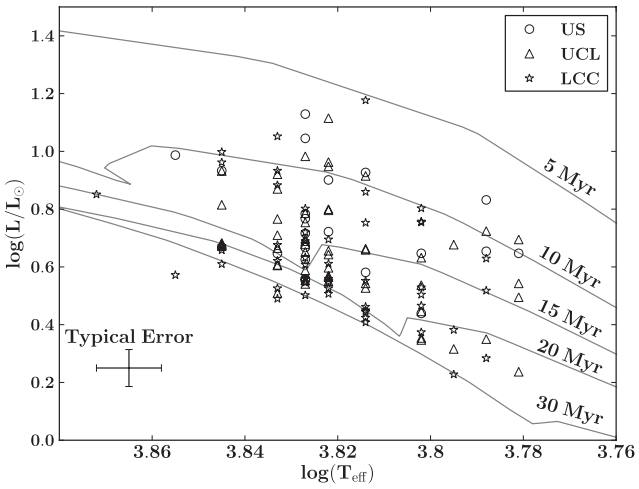

Figure 6. H-R diagram for all stars except identified interlopers. Circles, triangles, and star symbols are US, UCL, and LCC candidate members, respectively. Plotted for comparison are 5, 10, 15, 20, and 30 Myr isochrones from the Dotter et al. (2008) models.

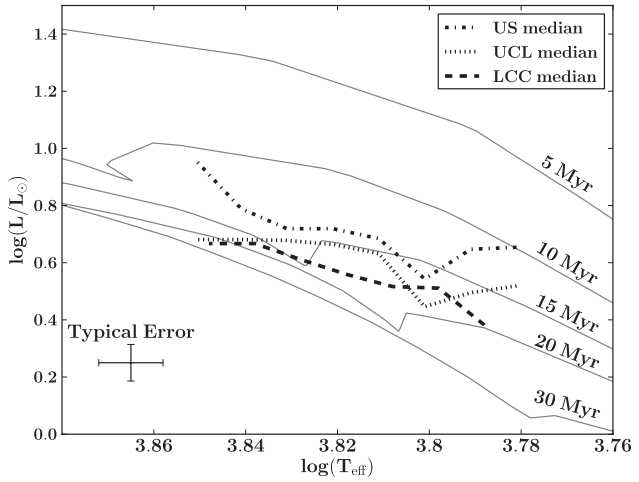

Figure 7. H-R diagram with empirical isochrones for US (dot-dashed), UCL (dotted), and LCC (solid), constructed by taking the median luminosity over a 0.01 dex $T_{\rm eff}$ step size with a 0.025 dex $\log(T_{\rm eff})$ window. Plotted for comparison are the Dotter et al. (2008) models.

theoretical H-R diagram. We compare our data to the Dartmouth PMS models (Dotter et al. 2008) in Figure 6.

5. DISCUSSION

Immediately noticeable in the H-R diagram (Figure 6) is that the Upper Sco F-stars are not clustered around the 5 Myr isochrone, the age often quoted for US (de Geus et al. 1989; Preibisch et al. 2002). In fact if a "moving median" empirical isochrone is plotted (Figure 7), it is ∼0.4 dex below the 5 Myr theoretical isochrone from the Dotter et al. (2008) models. While a choice of different theoretical tracks varies this disagreement slightly (e.g., D'Antona & Mazzitelli 1997; Siess et al. 2000; Demarque et al. 2004) the disparity is at least ∼0.4 dex at spectral type F3, which corresponds to a factor of $\gtrsim$2.5 in luminosity, or about 1 mag. This is such a large effect that it clearly cannot be attributed to the uncertainty in the photometry or the errors in spectral types.

Although there is some scatter, the positions of the empirical isochrones in Figure 7 are consistent with the age rank from previous results (Mamajek et al. 2002); from oldest to youngest: LCC, UCL, US. A close examination of the empirical isochrones reveals that UCL appears to be reaching the main sequence at $\log(T_{\rm eff}) \simeq 3.84$ or spectral type ∼F2, while LCC appears to be reaching the main sequence at $\log(T_{\rm eff}) \simeq 3.82$ or spectral type ∼F4. The F-type members of US appear to be all PMS, and thus we do not see a main-sequence turn-on point for US among F-type stars.

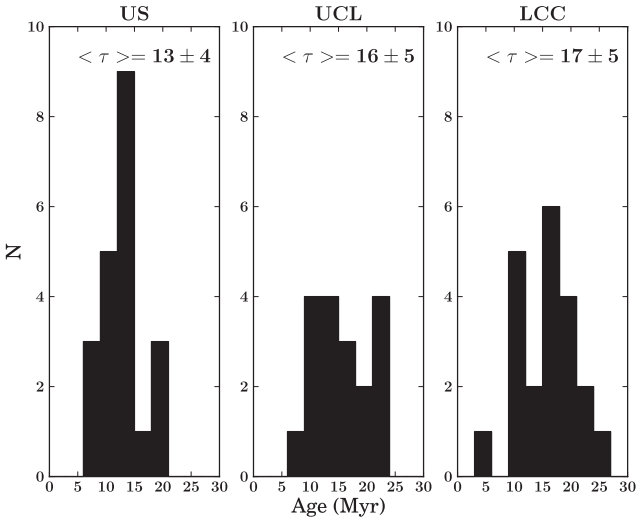

Figure 8. Distribution of ages obtained with the Dotter et al. (2008) evolutionary models. For UCL and LCC, only stars cooler than F5 were considered.

Table 6
Median Age Estimates of the PMS F-Type members of US, UCL, and LCC

Evolutionary Tracks	US (Myr)	UCL (Myr)	LCC (Myr)
Dartmouth	13 ± 4	16 ± 5	18 ± 7
Yonsei-Yale	13 ± 4	15 ± 5	18 ± 9
SDF00	14 ± 5	16 ± 9	15 ± 6
DM97	12 ± 3	15 ± 6	15 ± 5
Median	13	16	17
Statistical uncertainty	±1	±1	±1
Systematic uncertainty	±1	±1	±2

Notes. Uncertainties represent the 1σ dispersion in the Chauvenet's-criterion clipped ages (Bevington & Robinson 2003) for the members for which we were able to determine an age. The overall uncertainty is the 68% CL of the median (Gott et al. 2001) (statistical) and the dispersion in ages (systematic). Median ages for UCL and LCC are only defined by members F5 or cooler, as earlier members are too close to the main sequence to yield reliable ages.

5.1. Ages

For stars in UCL and LCC earlier than ∼F5, the H-R diagram positions of the stars are very near the main sequence and thus we cannot reliably determine ages from PMS evolutionary tracks. Therefore, we only use F5 and cooler stars to estimate the median age of UCL and LCC. For all stars in US and those later than F5 in UCL and LCC we calculate ages and masses by linearly interpolating between isochrones from Dotter et al. (2008), Demarque et al. (2004), Siess et al. (2000), and D'Antona & Mazzitelli (1997). Figure 8 shows the distribution of ages for the three subgroups. Individual results for our ages and masses are listed in Table 4. For stars which are too close to the main sequence to infer a reliable age, we determine a lower limit on the age using the 2σ upper limit on the luminosity and estimate a mass by assuming an age of 15 Myr (10 Myr for US). Our median age estimates for each subgroup are listed in Table 6.

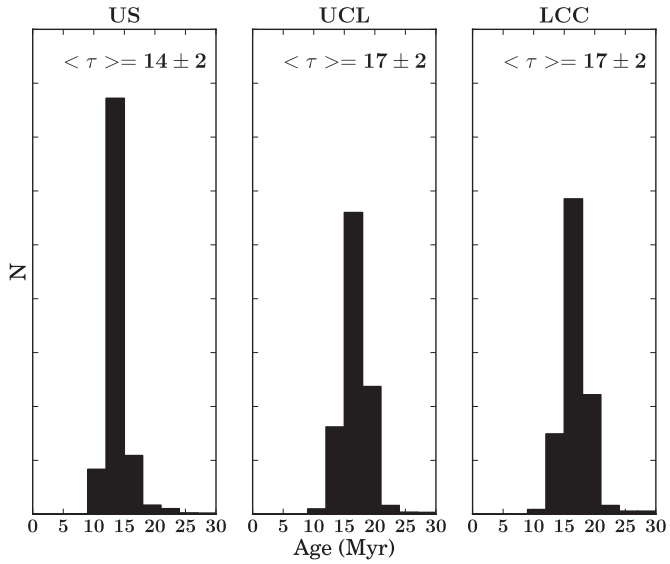

Figure 9. Distribution of ages obtained from a simulated population of 10^4 stars with median H-R diagram position and uncertainty with a Gaussian distribution (for UCL and LCC only members F5 or later were used). Ages (in Myr) were obtained using the Dotter et al. (2008) models.

Interestingly, we obtain a significantly older median age for Upper Sco than other studies of the low-mass members (5 Myr, Preibisch et al. 2002; 6–8 Myr, de Zeeuw & Brand 1985; 10 Myr, Glaspey 1971). As seen in Figure 8, we obtain a median age of 13 Myr for Upper Sco using the evolutionary tracks of Dotter et al. (2008) and an overall median age from all tracks of 13 ± 1 Myr (68% CL). This is disconcerting, especially considering that the median F-star ages we obtain for LCC and UCL are consistent with the main-sequence turnoff ages and the PMS G- and K-type stars examined in Mamajek et al. (2002). Motivated to resolve this large discrepancy, we revisit the Upper Sco main-sequence turnoff ages, the age of the M supergiant Antares, examine the ages of the A-type stars and the ages for the PMS G-type stars. We also examine a kinematic expansion age for Upper Sco.

5.1.1. Intrinsic Age Spreads

In order to constrain how much of the observed spread in ages is due to observational uncertainty and estimate the intrinsic age spread, we performed a simple Monte Carlo simulation. First we calculated the observed 1σ dispersion in ages for each subgroup by simply taking the standard deviation of the ages (F5 and later stars for UCL and LCC), with deviant outliers clipped using Chauvenet's criterion (Bevington & Robinson 2003). These observed spreads are shown in Table 6.

For each subgroup, we generated a synthetic population of 10^4 H-R diagram positions using the median H-R diagram position and median uncertainties for our member stars (F5 or later only for UCL and LCC), assuming a Gaussian distribution of errors. We then obtained ages and calculated the 1σ spread in ages for these three synthetic populations, again clipping deviant outliers with Chauvenet's criterion since the same criterion was applied to our real data to obtain the 1σ dispersion in ages. The distribution of ages for these simulated populations with the Dotter et al. (2008) evolutionary tracks is shown in Figure 9.

Our estimates here assume that the observed dispersion in ages is the result of the true dispersion in ages and the dispersion in ages as a result of the observational uncertainties, i.e., $\sigma^2_{\rm observed} = \sigma^2_{\rm intrinsic} + \sigma^2_{\rm uncertainties}$. Using the Dotter et al. (2008) models, we then estimate the intrinsic dispersion in ages using the dispersions from our real and simulated populations. Rather than give preference to one set of evolutionary models, we repeat this calculation for each of our evolutionary models. This way we obtain a range of intrinsic age dispersions.

For US the observed 1σ dispersion in ages ranges from ±3 Myr with the D'Antona & Mazzitelli (1997) models to ±5 Myr with the Siess et al. (2000) models. When we account for the age dispersion from the observational uncertainties, we find the intrinsic 1σ age dispersion ranges from ±1 Myr to ±3 Myr, again depending on the models. For UCL and LCC, which have an observed age dispersion of ±5–9 Myr and ±5–9 Myr (depending on models), we find intrinsic age dispersions of ±4–7 Myr and ±0–8 Myr, respectively. This indicates that 68% of the star formation in Sco-Cen occurred over a time span of 2–6 Myr (US), 8–14 Myr (UCL), and <16 Myr (LCC). These are upper limits as we have not accounted for stellar binarity. Our findings show a much smaller age dispersion for US than the other two subgroups, consistent with the smaller age spreads found by Preibisch et al. (2002) and Slesnick et al. (2008), who also found a very small intrinsic dispersion in age. For UCL and LCC our age spreads are larger than that found in Mamajek et al. (2002), who found that 68% of the star formation had occurred within 4–6 Myr for UCL and LCC.

5.2. Upper Sco Main-sequence Turnoff Revisited

The most recent age determination for the turnoff was performed by de Geus et al. (1989) using Walraven photometry in which they estimated a turnoff age of 5 Myr using Maeder (1981) evolutionary tracks with overshooting but no mass loss or rotation. Preibisch et al. (2002) examined the H-R diagram again and argued that the data were consistent with an age of 5 Myr with very little spread in ages. We now have updated stellar evolutionary models and *Hipparcos* astrometry which we employ to revisit the turnoff age. We use the early-type members from de Zeeuw et al. (1999) with the addition of δ Sco, a long-period binary that is certainly a member of US but was not a de Zeeuw et al. (1999) member of US due to its perturbed motion. To construct the H-R diagram, we take Strömgren photometry from Hauck & Mermilliod (1998) and de-redden it according to the prescription of Shobbrook (1983). We then use the $T_{\rm eff}$ and BC_V calibration of Balona (1994) with the de-reddened Strömgren photometry. Since we are using the spread in isochrones near where the stars evolve off the main sequence, we restrict ourselves to stars hotter than $\log(T_{\rm eff}) > 4.40$ dex or more luminous than $\log(L/L_\odot) > 4.00$ dex. For stars cooler or less luminous than this the derived ages are very sensitive to the observational uncertainties and we are unable to estimate meaningful ages. Our derived temperatures and luminosities are given in Table 7. A plot of the data, with and without corrections for binarity (see below), is shown in Figure 10 with the evolutionary tracks of Bertelli et al. (1994).

We have not used the runaway star ζ Oph in our analysis, for several reasons. First, while Hoogerwerf et al. (2000) used *Hipparcos* astrometry to conclude that ζ Oph most likely originated from Upper Sco ∼1 Myr ago, they note that it could have also originated from UCL ∼3 Myr ago. Unfortunately, the radial velocity of this star is poorly constrained[10] and thus the UVW space motion is not sufficiently constrained to associate

[10] +15 km s^{-1}, Reid et al. (1993); +6 km s^{-1}, Garmany et al. (1980); −12.6 km s^{-1}, Conti et al. (1977); −15 km s^{-1}, Valdes et al. (2004).

Table 7
Stellar Parameters for US Turnoff Stars

Name	$\log(T_{\rm eff})$ (dex)	$\log(L/L_{\odot})$ (dex)	$v \sin i$ (km s^{-1})	B94 Age (Myr)	B94 Mass ($M_{\odot}$)	E11 Age (no rot.) (Myr)	E11 Mass (no rot.) ($M_{\odot}$)	E11 Age (rot.) (Myr)	E11 Mass (rot.) ($M_{\odot}$)
ω Sco	4.424 ± 0.019	3.96 ± 0.05	100 ± 6	2	11.4	5	11.2	5	11.4
β^1 Sco	4.419 ± 0.010	4.29 ± 0.05	91 ± 8	9	12.2	11	12.1	11	12.2
π Sco	4.402 ± 0.007	4.34 ± 0.10	100 ± 15	12	12.4	12	12.9	14	12.6
τ Sco	4.475 ± 0.073	4.31 ± 0.16	10 ± 2	2	14.7	5	14.5	5	14.7
δ Sco	4.438 ± 0.033	4.58 ± 0.14	148 ± 8	9	14.4	9	14.9	10	14.6
σ Sco	4.443 ± 0.015	4.98 ± 0.12	56 ± 15	8	17.7	8	18.0	10	17.2

References. (B94) Bertelli et al. 1994; (E11) Ekström et al. 2011. $v \sin i$ values adopted from Brown & Verschueren (1997).

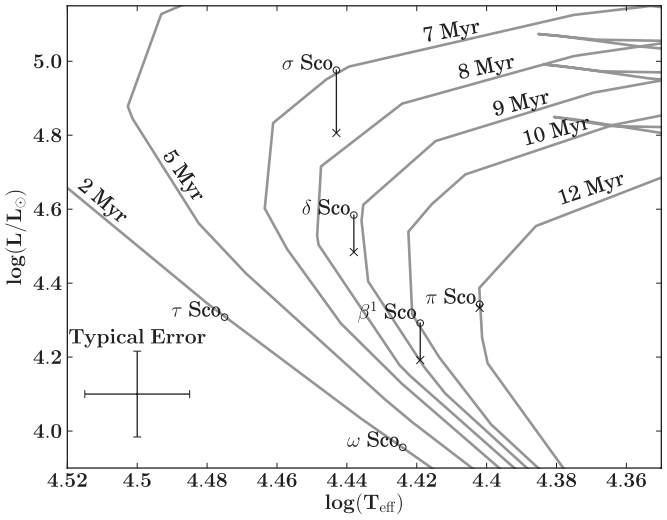

Figure 10. Upper Sco main-sequence turnoff plotted with the Bertelli et al. (1994) evolutionary tracks. The crosses represent the H-R diagram position corrected for known binarity (see the text for a discussion of each binary). The circles are the H-R diagram positions uncorrected for companions. ω Sco and τ Sco do not have known companions.

it with Upper Sco with great confidence. More importantly, however, a close examination of the abundance patterns in ζ Oph indicates that it has an anomalously high helium abundance (Herrero et al. 1992) and thus likely participated in a mass transfer event, perhaps from a close former binary companion. For this reason it is not reliable to use it to determine the turnoff age since it may have received extra nuclear fuel unaccounted for by the evolutionary models.

With only six B-type stars determining the turnoff age, it is important to assess the binarity of these stars since it may significantly alter the H-R diagram positions and, therefore, the derived ages. Only two stars, ω Sco and τ Sco, do not have a detected companion. β^1 Sco is a binary with $\Delta V = 1.26 \pm 0.17$ (Elliot et al. 1976). This magnitude shift, when accounted for, moves the primary down on the H-R diagram $\sim$0.1 dex in luminosity and gives an age for the primary of 9 Myr. π Sco is a binary with $\Delta V \sim 3.7$ (Stickland et al. 1996), which moves the primary down on the H-R diagram $\sim$0.01 dex in luminosity, having virtually no effect on the derived age for π Sco. δ Sco is a binary with $\Delta V = 1.5$–1.9 (Tango et al. 2009), shifting the primary down $\sim$0.07–0.1 dex in luminosity. However, because of its position it effectively moves parallel to the 9 Myr isochrone and thus does not affect the derived age for the primary. σ Sco is a quadruple system discussed extensively by North et al. (2007). They report the system as a spectroscopic pair (which includes the primary), a tertiary B7 component, and a B9.5V common proper motion companion separated by 20″. They deconstructed the spectroscopic pair into a B1III primary with a B1V secondary with $\Delta V \simeq 0.80$, and a system age of $\sim$10 Myr using the Claret (2004) evolutionary models. Correcting our derived H-R diagram position for the magnitude of the secondary, we find that the primary moves down $\sim$0.2 dex, which changes our derived age to 8 Myr for the primary.

Unfortunately, the massive stars in US do not trace a well-defined turnoff, even with corrections for known companions. Including the shifted H-R diagram positions when accounting for the binarity, we estimate the turnoff age from the following stars: ω Sco (2 Myr), τ Sco (2 Myr), β^1 Sco (9 Myr), δ Sco (9 Myr), π Sco (12 Myr), and σ Sco (8 Myr). The median age for these stars is 9 ± 3 Myr (68% CL) with 1σ dispersion 4 Myr, midway between the previous age estimates of $\sim$5 Myr and our value of $\sim$13 Myr from the F-type members.

While most current stellar evolutionary models have ignored rotation, theoretical studies have shown that a moderate rotational velocity of $v_{\rm eq} \sim 200$ km s^{-1} will increase main-sequence lifetimes about 20%–30% (Meynet & Maeder 2000; Maeder & Meynet 2000; Talon et al. 1997). This represents a significant difference in ages obtained with evolutionary tracks ignoring rotation versus those which include a treatment of rotation. For this reason, we also considered the evolutionary tracks of Ekström et al. (2011) which include tracks for stars with and without rotation. It should be noted that neither the Bertelli et al. (1994) models nor the Ekström et al. (2011) models considered here include PMS evolution, but since the PMS evolution for a $\sim 9\,M_{\odot}$ star is $\sim 10^5$ yr (Iben 1965) the PMS time can be safely neglected. Plotted in Figure 11 are the H-R diagram positions of the US main-sequence turnoff stars along with isochrones generated from the evolutionary tracks of Ekström et al. (2011) with no rotation (dashed lines) and those with a rotational velocity equal to 40% of the breakup velocity. The median age with rotation at 40% of breakup is 10 ± 2 Myr (68% CL) while the median age without is 9 ± 2 Myr (68% CL). Since the US turnoff stars are rotating with a median projected rotational velocity of $\langle v \sin i \rangle = 96$ km s^{-1} (see Table 7) and $\langle v_{\rm eq} \rangle = (4/\pi)\langle v \sin i \rangle$, then the turnoff stars have $\langle v_{\rm eq} \rangle \simeq 120$ km s^{-1}. Using mass estimates from the Bertelli et al. (1994) tracks, we estimate the median break-up velocity of the US turnoff stars as $\sim$450 km s^{-1} and thus the median observed rotational velocity is $\sim$25% of breakup. This is a significant median rotational velocity and indicates that rotation should be considered. Therefore we adopt the median age obtained with the rotating evolutionary tracks of 10 ± 2 Myr (68% CL).

Our Upper Sco turnoff age is much older than the age derived by the de Geus et al. (1989) study. We believe that the major

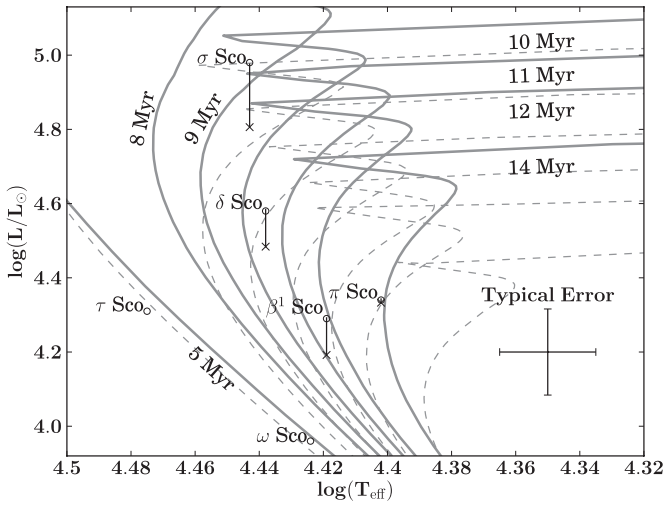

Figure 11. Upper Sco main-sequence turnoff plotted with the Ekström et al. (2011) evolutionary tracks without rotation (dashed lines) and with $v = 0.4\ v_{\rm breakup}$ (solid lines). The crosses and circles represent the H-R diagram positions corrected and uncorrected for known binarity, respectively.

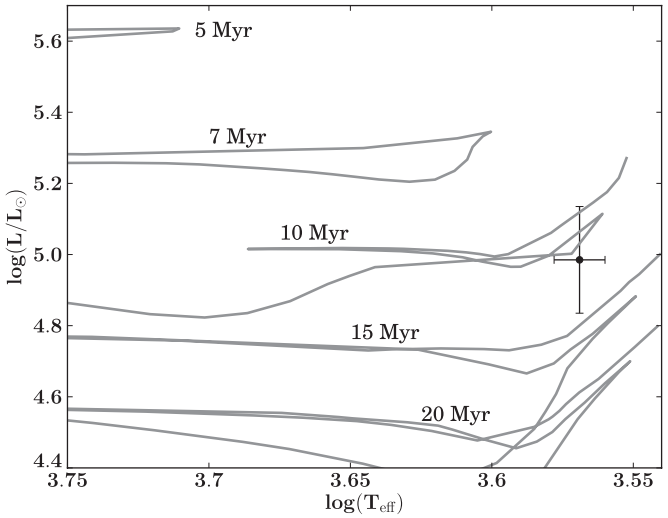

Figure 12. H-R diagram for M1.5Iab-Ib supergiant Antares (α Sco). The theoretical isochrones overlap in this region, but the best fit is 11^{+3}_{-1} Myr using Bertelli et al. (1994) evolutionary tracks.

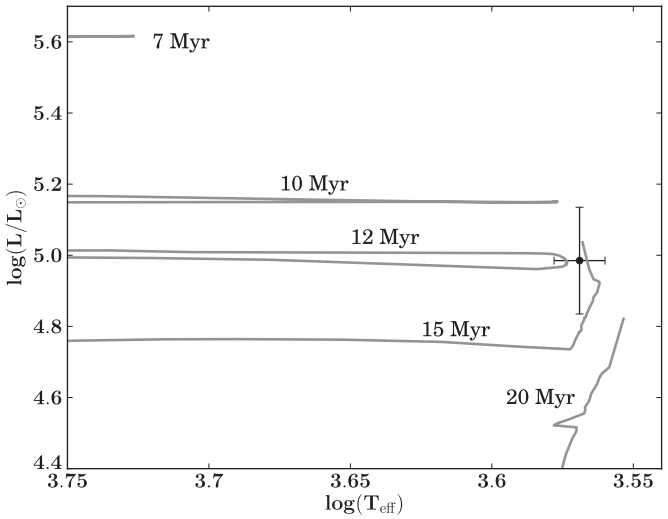

Figure 13. H-R diagram for Antares with the rotating evolutionary tracks of Ekström et al. (2011). We adopt a final age of Antares of 12^{+3}_{-1} Myr.

source of discrepancy between the de Geus et al. (1989) US turnoff ages and our US turnoff ages is the updated evolutionary tracks. If we use the de Geus et al. (1989) H-R diagram positions with the Bertelli et al. (1994) evolutionary tracks, we obtain a median age of 9 Myr, the same age we obtain with our modern data (though our individual H-R diagram positions are not the same as those in the de Geus et al. 1989 study). We also note that the use of evolutionary tracks which account for rotation tends to increase the derived ages by ∼25% in general (Meynet & Maeder 2000). For example, using the Ekström et al. (2011) rotating evolutionary tracks for a typical upper main-sequence star in LCC and UCL gives an age ∼30% older than ages derived with the Bertelli et al. (1994) evolutionary tracks. Revisiting the turnoff ages for UCL and LCC is beyond the scope of this paper, but may be considered in a future paper.

5.3. Antares

Antares (α Sco) is a rare M1.5Iab-Ib supergiant (Keenan & McNeil 1989) in US. As the most massive secure member of US, it places tight constraints on the age of the group. To estimate the H-R diagram of Antares we use the updated temperature scale of Levesque et al. (2005) for red supergiants, together with the revised *Hipparcos* parallax (van Leeuwen 2007) of $\pi = 5.89 \pm 1.00$ mas and the angular diameter measurement of 41.3 ± 1.0 mas (Richichi & Lisi 1990). We obtain $\log(T_{\rm eff}) = 3.569 \pm 0.009$ dex (assuming spectral type uncertainty of 1 subtype), $\log(L/L_{\odot}) = 4.99 \pm 0.15$ dex. This H-R diagram position is plotted in Figure 12. With this H-R diagram position we obtain an initial mass of 16.6 $M_{\odot}$ and an age of 11^{+3}_{-1} Myr with the evolutionary tracks of Bertelli et al. (1994). However, just as with the main-sequence turnoff stars, the main-sequence lifetime of Antares was likely significantly altered by rotation and therefore we again consider the rotating evolutionary tracks of Ekström et al. (2011), shown in Figure 13. From these rotating evolutionary tracks we obtain an initial mass of 17.2 $M_{\odot}$ and an age of 12^{+3}_{-1} Myr, which we adopt as our final age for Antares.

However, independent of this H-R diagram position we can still place constraints on the age of Antares using only the $T_{\rm eff}$ derived from the spectral type. Using the previously mentioned $T_{\rm eff}$ calibration for supergiants, a $T_{\rm eff}$ of 3710 K ($\log(T_{\rm eff}) = 3.569$) means that the age must be 9 Myr or more, since younger isochrones are not predicted to reach temperatures that low. This is illustrated in Figure 12 with the placement of the 5 Myr isochrone to the left.

5.4. Ages of Upper Sco A-Type Stars

We place the A-type stars of US on the H-R diagram as another independent age indicator. The F-type stars do not appear to be reaching the main sequence and thus we expect that some A-type stars will be PMS and therefore useful as an age indicator.

We use the kinematically selected A-type US members of de Zeeuw et al. (1999) and perform essentially the same analysis as used on the F-type stars. We estimate individual reddenings using the procedure described in Section 4.2. We calculate a kinematic parallax, again using the revised *Hipparcos* astrometry if the solution is that of a single star and use the *Tycho-2* proper motions otherwise. We reject one star, HIP 77457, since its trigonometric parallax of 8.58 ± 0.86 mas disagrees with the kinematic parallax of 5.10 ± 0.42 mas by more than 3σ. Our individual H-R diagram position data for the US A-type stars

Table 8
Stellar Parameters For A-type Upper Sco Members

HIP	Spectral Type	A_V (mag)	$\pi_{\rm kin}$ (mas)	$\log(T_{\rm eff})$ (dex)	$\log(L/L_\odot)$ (dex)	References
76310	A0V	0.14 ± 0.03	8.22 ± 0.62	3.980 ± 0.031	1.271 ± 0.070	1
77545	A2/3V	1.25 ± 0.04	6.83 ± 0.62	3.937 ± 0.014	1.053 ± 0.081	2
77815	A5V	0.85 ± 0.07	6.89 ± 0.58	3.907 ± 0.007	1.195 ± 0.077	2
77960	A4IV/V	0.75 ± 0.02	8.56 ± 0.71	3.918 ± 0.012	0.973 ± 0.093	2
78099	A0V	0.59 ± 0.03	7.42 ± 0.59	3.980 ± 0.031	1.367 ± 0.073	2
78196	A0V	0.00 ± 0.04	8.45 ± 0.63	3.980 ± 0.031	1.302 ± 0.070	3
78494	A2mA7-F2	0.75 ± 0.06	7.26 ± 0.57	3.943 ± 0.016	1.395 ± 0.077	2
78809	A1Vnn	0.21 ± 0.05	7.29 ± 0.57	3.964 ± 0.019	1.244 ± 0.071	1
78847	A0V	0.63 ± 0.06	6.76 ± 0.55	3.980 ± 0.031	1.445 ± 0.078	1
78963	A9V	0.64 ± 0.06	5.11 ± 0.46	3.872 ± 0.010	1.314 ± 0.084	3
78996	A9V	0.47 ± 0.03	7.25 ± 0.57	3.872 ± 0.010	1.019 ± 0.069	2
79124	A0V	0.78 ± 0.05	6.51 ± 0.53	3.980 ± 0.031	1.550 ± 0.078	2
79156	A0V	0.60 ± 0.07	6.43 ± 0.54	3.980 ± 0.031	1.366 ± 0.081	1
79250	A3III/IV	0.33 ± 0.05	9.60 ± 0.75	3.932 ± 0.012	0.963 ± 0.072	2
79366	A3V	0.80 ± 0.02	7.35 ± 0.60	3.932 ± 0.012	1.202 ± 0.071	2
79392	A2IV	0.71 ± 0.04	5.81 ± 0.49	3.943 ± 0.016	1.300 ± 0.076	2
79476	A8IVe	1.02 ± 0.40	7.56 ± 0.61	3.875 ± 0.010	1.006 ± 0.175	4
79733	A1mA9-F2	1.25 ± 0.04	4.51 ± 0.43	3.964 ± 0.019	1.480 ± 0.092	3
79860	A0V	0.38 ± 0.03	4.91 ± 0.40	3.980 ± 0.031	1.432 ± 0.075	3
79878	A0V	0.00 ± 0.02	7.35 ± 0.55	3.980 ± 0.031	1.407 ± 0.070	5
79987	A7V	1.69 ± 0.18	3.84 ± 0.40	3.892 ± 0.014	1.308 ± 0.116	6
80019	A0V	1.03 ± 0.07	7.81 ± 0.68	3.980 ± 0.031	1.374 ± 0.084	1
80059	A7III/IV	0.56 ± 0.07	7.74 ± 0.64	3.892 ± 0.014	0.907 ± 0.075	2
80088	A9V	0.61 ± 0.03	6.11 ± 0.66	3.872 ± 0.010	0.960 ± 0.095	2
80130	A9V	0.66 ± 0.02	6.41 ± 0.57	3.872 ± 0.010	1.089 ± 0.077	2
80196	A1Vn	2.36 ± 0.18	5.94 ± 0.56	3.964 ± 0.019	1.602 ± 0.102	6
80238	A2.5V	0.74 ± 0.09	8.00 ± 0.68	3.937 ± 0.014	1.389 ± 0.081	7
80311	A1V	0.93 ± 0.05	5.51 ± 0.49	3.964 ± 0.019	1.266 ± 0.080	6
80425	A1V	1.52 ± 0.17	7.25 ± 0.64	3.964 ± 0.019	1.392 ± 0.096	6
80799	A3V	0.25 ± 0.04	7.97 ± 0.62	3.932 ± 0.012	1.078 ± 0.068	6
81624	"A3*"	2.56 ± 0.78	5.08 ± 0.48	3.932 ± 0.012	2.003 ± 0.316	8
82397	A3V	0.00 ± 0.03	7.85 ± 0.62	3.932 ± 0.012	1.118 ± 0.072	3

Notes. Uncertainties in $\log(T_{\rm eff})$ are determined assuming a spectral type uncertainty of 1 subtype. Spectral type references: (1) Paunzen et al. 2001; (2) Houk & Smith-Moore 1988; (3) Houk 1982; (4) Vieira et al. 2003; (5) Glaspey 1972; (6) Garrison 1967; (7) Abt 1981; (8) Gray & Corbally 1998. *We list the hydrogen type in the table, the full type from Gray & Corbally (1998) is "kA1 hA3 mA3 Vaer Bd1 $\leqslant$ Nem1."

Table 9
Age Constraints for Upper Sco from the A-type Main-Sequence Turn-on

Evolutionary Tracks	Age (Myr)
Dartmouth	10 ± 2
Yonsei-Yale	10 ± 2
SDF00	12 ± 3
DM97	9 ± 2
Median	10
Statistical uncertainty	± 1
Systematic uncertainty	± 1

Notes. The overall uncertainty is the 68% CL of the median (Gott et al. 2001) (statistical) and the dispersion in ages (systematic).

are listed in Table 8 and plotted in Figure 14. As with the F-type stars, we do not see the A-type stars clustered around the 5 Myr isochrone, but rather mostly between the 5 Myr and 12 Myr isochrones.

While the A-type stars in US have individual H-R diagram positions that are too close to the main sequence to yield reliable ages, we can examine the trend of the empirical isochrone and determine what ages are consistent with the ensemble. Shown in Figure 14 is the empirical isochrone, which we use to estimate the main-sequence turn-on for Upper Sco at spectral type ~A3 or $\log(T_{\rm eff}) \simeq 3.93$ dex. We compare our empirical isochrones with the Dotter et al. (2008) evolutionary models, noting that an age of 8 Myr is too young to be consistent with the clump of stars at spectral type A3, and an age of 12 Myr is too old to be consistent with the clump of stars at spectral type A8–A9. Using these constraints, we estimate an age of 10 ± 2 Myr with the Dotter et al. (2008) evolutionary tracks. We obtain similar age estimates with other evolutionary models, summarized in Table 9. For the A-type stars we adopt the median age among all four evolutionary models considered of $10 \pm 1 \pm 1$ Myr (statistical, systematic).

5.5. Ages of Upper Sco Pre-main Sequence G-type Stars Revisited

Since our F-type median ages for LCC and UCL agree very well with previous results obtained with the G-type PMS (Mamajek et al. 2002), we wish to directly compare our new results for US with a similar sample of G-type stars in an attempt to resolve this discrepancy in ages. We use the X-ray-selected G-type stars from Preibisch & Zinnecker (1999) and the kinematically selected G-type stars from de Zeeuw et al.

Table 10
Stellar Parameters for G-Type Upper Sco Members

Object	TYC	SpT	$\pi_{\rm kin}$ (mas)	A_V (mag)	$\log(T_{\rm eff})$ (dex)	$\log(L/L_\odot)$ (dex)	D08 (Myr)	YY04 (Myr)	S00 (Myr)	DM97 (Myr)	References
[PZ99] J155548.7-251223	6783-2045-1	G3	6.56 ± 0.85	0.70 ± 0.17	3.756	0.38 ± 0.13	11	12	18	12	(1)
[PZ99] J161618.0-233947	6793-1406-1	G7	7.17 ± 0.81	0.73 ± 0.06	3.742	0.34 ± 0.10	9	10	16	9	(1)
[PZ99] J160843.4-260216	6784-39-1	G7	7.39 ± 0.66	0.65 ± 0.09	3.742	0.36 ± 0.09	9	10	15	9	(1)
[PZ99] J161459.2-275023	6801-186-1	G5	7.66 ± 0.92	0.73 ± 0.31	3.750	0.08 ± 0.16	23	23	30	21	(1)
[PZ99] J160040.6-220032	6212-1183-1	G9	6.36 ± 1.06	0.65 ± 0.17	3.728	0.27 ± 0.16	8	9	15	7	(1)
[PZ99] J160000.7-250941	6783-1747-1	G0	6.86 ± 0.65	0.36 ± 0.19	3.774	0.19 ± 0.11	24	24	...	22	(1)
[PZ99] J160158.2-200811	6208-1543-1	G5	6.31 ± 0.77	1.22 ± 0.25	3.750	0.65 ± 0.15	5	6	10	5	(1)
[PZ99] J155812.7-232835	6779-780-1	G2	6.60 ± 0.77	0.86 ± 0.18	3.762	0.49 ± 0.12	10	10	16	10	(1)
[PZ99] J161731.4-230334	6793-501-1	G0	5.37 ± 0.78	0.72 ± 0.15	3.774	0.71 ± 0.14	8	8	12	8	(1)
[PZ99] J161318.6-221248	6213-306-1	G9	6.90 ± 0.75	1.16 ± 0.16	3.728	0.60 ± 0.12	4	4	7	4	(1)
HIP 78483	6787-1367-1	G2IV	6.46 ± 0.61	0.22 ± 0.12	3.762	0.64 ± 0.10	7	8	12	7	(2)
HIP 78581	7329-1646-1	G1V	9.26 ± 0.75	0.04 ± 0.06	3.769	0.38 ± 0.08	15	15	20	15	(3)
HIP 79252	6213-75-1	G7IV(e)	8.94 ± 0.86	0.64 ± 0.23	3.742	0.45 ± 0.12	7	8	13	7	(2)
HIP 79462	6793-1271-1	G2V	7.03 ± 0.61	0.45 ± 0.15	3.762	0.70 ± 0.10	6	7	10	7	(4)
HIP 80320	6806-833-1	G3IV	7.97 ± 0.63	0.00 ± 0.04	3.756	0.42 ± 0.07	10	11	17	11	(2)
HIP 80535	6802-183-1	G0V	7.59 ± 0.64	0.00 ± 0.02	3.774	0.71 ± 0.07	8	8	12	8	(3)

Notes. Spectral type references: (1) Preibisch & Zinnecker 1999; (2) Torres et al. 2006; (3) Houk 1982; (4) Houk & Smith-Moore 1988.

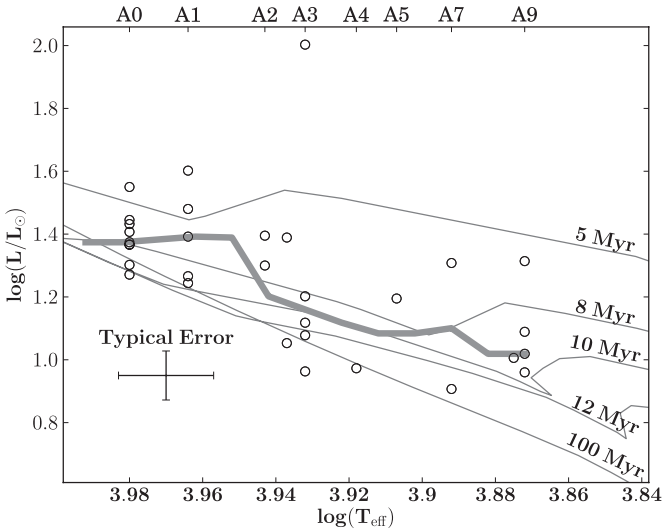

Figure 14. H-R diagram for Upper Sco A-type stars taken from de Zeeuw et al. (1999). Plotted for comparison are 5, 8, 10, 12, and 100 Myr isochrones (solid lines) from the Dotter et al. (2008) models. The star well above the 5 Myr isochrone is HD 150193 (HIP 81624), a known Herbig Ae/Be star (Hernández et al. 2005). While situated in de Zeeuw et al's Upper Sco "box," it appears to be associated with the Oph filamentary clouds L1729 and 1712, far from most of the other Upper Sco members. The thick solid line is an empirical isochrone constructed by taking the median luminosity over a 0.01 dex $T_{\rm eff}$ step size with a 0.035 dex window. Uncertainties in $\log(T_{\rm eff})$ are determined assuming a spectral type uncertainty of 1 subtype.

(1999). Ages for the X-ray-selected objects from the Preibisch & Zinnecker (1999) study had been estimated previously using UKST Schmidt plate photometry. However, more precise *Tycho-2* and 2MASS photometry are now available and thus we may be able to obtain a more reliable age estimate. Ages for the US G-type stars in the de Zeeuw et al. (1999) sample have not been previously examined.

For the X-ray-selected sample we cross-reference the Preibisch & Zinnecker (1999) sample with the *Tycho-2* catalog (Høg et al. 2000) and select objects which have proper motions within the de Zeeuw et al. (1999) proper motion boundaries for Upper Sco (i.e., 0 mas yr^{-1} $< \mu <$ 37 mas yr^{-1}). This leaves us with 10 X-ray-selected G-type US members. We correct for extinction using $(B-V)$, $(V-J)$, $(V-H)$, and $(V-K)$ colors from *Tycho-2* and 2MASS photometry, with the *Tycho-2* photometry converted to Johnson using the conversions found in Mamajek et al. (2002, 2006). To estimate bolometric luminosity we use the converted V-band photometry, kinematic distances using the *Tycho-2* proper motions and temperatures and bolometric corrections listed in Table 3. For the kinematically selected sample, we first identify two interlopers, HIP 83542 and HIP 81392. Houk & Smith-Moore (1988) classified HIP 83542 as G8/K0 III, a giant, and the H-R diagram position is well above the 1 Myr isochrones, consistent with this assessment. HIP 81392 and HIP 83542 both exhibit weak lithium absorption features, significantly lower than the other six kinematically selected US candidates from de Zeeuw et al. (1999) and inconsistent with the youth of Upper Sco (E. Mamajek 2011, private communication). With these interlopers removed, we are then left with six G-type US members from de Zeeuw et al. (1999). For the de Zeeuw et al. (1999) G-type US candidate members we estimate extinction, $T_{\rm eff}$, distance, and bolometric luminosity using the same method as for the F-type stars as previously discussed. Our newly derived extinctions, distances, and H-R data are listed in Table 10, with the H-R diagram for this analysis shown in Figure 15.

For the 16 G-type members of Upper Sco described above, we find median ages of 8–14 Myr using the evolutionary tracks of Dotter et al. (2008), Demarque et al. (2004), Siess et al. (2000), and D'Antona & Mazzitelli (1997). Our derived ages for these G-type stars of Upper Sco are summarized in Table 11, with an overall median age among all tracks of $9 \pm 2 \pm 3$ Myr (statistical, systematic). The kinematically selected members are slightly more biased toward younger ages than the X-ray-selected members. However, this slight difference may be attributed to the brightness limits of the *Hipparcos* catalog. The difference may not be significant, though, with such small numbers of members.

5.6. Upper Sco Expansion Age

One of the earlier published ages for US is an expansion age of ~5 Myr derived by Blaauw (1978). Deriving ages

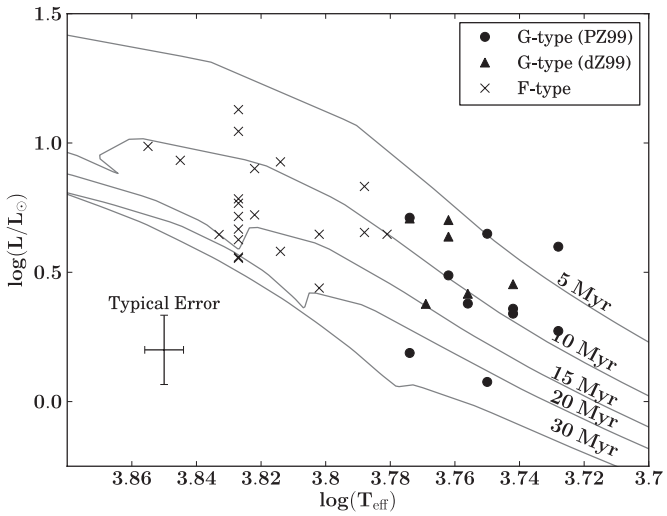

Figure 15. H-R diagram for Upper Sco G-type stars taken from Preibisch & Zinnecker (1999) (solid triangles) and de Zeeuw et al. (1999) (solid circles) with *Tycho*-2 proper motions within the de Zeeuw et al. (1999) boundaries. F-type members (this work) are shown for continuity (crosses). Plotted for comparison are 5, 10, 15, 20, and 30 Myr isochrones from the Dotter et al. (2008) models.

using kinematic data holds obvious appeal since it does not depend on stellar evolution models. However, Brown et al. (1997), performing simulations of expanding OB associations and analyzing the resulting simulated proper motion data, found major problems with kinematic expansion ages which only rely on proper motion data. They found that expansion ages determined by tracing the proper motion of the stars back to their smallest configuration, as was performed in Blaauw (1978) to obtain the often quoted age of 5 Myr for US, always lead to underestimated ages and that all age estimates converge to ~4 Myr. Furthermore, they found that the initial size of the OB association provided by this method is always overestimated. The Brown et al. (1997) study found that kinematic expansion ages determined using proper motion data alone are essentially meaningless.

Radial velocities must be considered in order to derive a meaningful expansion age. Given the availability of good quality trigonometric parallax and radial velocity data and the findings of Brown et al. (1997), we revisit the expansion age for US here. Following Mamajek (2005), we adopt a Blaauw expansion model (Blaauw 1956, 1964) which gives the observed radial velocity for parallel motion as

$$v_{\rm obs} = v' \cos\lambda + \kappa r + K,$$

where v' is the centroid speed of the group, λ is the angular distance to the convergent point, $v' \cos\lambda = v_{\rm pred}$ is the predicted radial velocity with no expansion, κ is the expansion term in units of km s^{-1} pc^{-1}, r is the distance to the star in pc, and K is an offset term which may include intrinsic effects (e.g., convective blueshift or gravitational redshift). We then write the difference between the predicted and observed radial velocities as

$$v_{\rm obs} - v_{\rm pred} = \Delta V_R = \kappa r + K$$

so that κ is the slope in the plot of ΔV_R versus r:

$$\kappa = \frac{d(\Delta V_R)}{dr}.$$

Table 11
Median Ages of the G-Type Upper Sco Members

Evolutionary Tracks	Age (Myr)
Dartmouth	8 ± 4
Yonsei-Yale	9 ± 3
SDF00	14 ± 4
DM97	8 ± 4
Median	9
Statistical uncertainty	± 2
Systematic uncertainty	± 3

Notes. Uncertainties represent the 1σ dispersion in the Chauvenet's-criterion clipped ages (Bevington & Robinson 2003). The uncertainty in the median is the 68% confidence limit as described in Gott et al. (2001) (statistical) and the dispersion in ages (systematic).

The expansion age in Myr is then

$$\tau = \gamma^{-1}\kappa^{-1},$$

where $\gamma = 1.0227$ pc s Myr^{-1} km^{-1}, a conversion factor.

To determine the expansion age we have started with the entire de Zeeuw et al. (1999) sample for which radial velocity measurements were available in the literature (listed in Table 12), since these all have individual trigonometric parallaxes. We have used radial velocities from Dahm et al. (2011), Chen et al. (2011), Gontcharov (2006), and Duflot et al. (1995). We limited the sample to those de Zeeuw et al. (1999) candidate members which have revised *Hipparcos* distances (van Leeuwen 2007)[11] within 50 pc of the mean US distance (145 pc; de Zeeuw et al. 1999). We also excluded candidate members with radial velocities more than 20 km s^{-1} discrepant from the predicted radial velocities, as these are almost certainly non-members or unresolved binaries. Our $v_{\rm pred}$ is calculated using the new best estimate of the mean UVW motion of Upper Sco, detailed in Chen et al. (2011). The one-dimensional velocity dispersion in US is 1.3 km s^{-1} (de Bruijne 1999b). In order to determine if there is evidence of expansion, we plot the distance r versus ΔV_R in Figure 16. Expansion would be exhibited by a positive correlation between the distance and ΔV_R, characterized by the slope (κ) of a line fit to the data. To take into account the observational errors in distance and radial velocity in fitting a line to the data, we performed a Monte Carlo simulation in which we added random Gaussian errors commensurate with each observational error to the observed data point, and then we fit a line using an unweighted total least squares algorithm. We performed 50,000 trials and then used the median and 1σ spread to quantify the effect of the uncertainties in the observational data on the slope. This yielded a Pearson r of -0.03 ± 0.11 and a best-fit line with a slope of $\kappa = -0.01 \pm 0.04$ km s^{-1} pc^{-1}. If we consider only models of expansion (i.e., $\kappa > 0$), then the 99% confidence lower limit on the expansion age is 10.5 Myr. However, the *results are statistically consistent with no expansion*. For an expansion age of 5 ± 2 Myr we would expect $\kappa = 0.20^{+0.13}_{-0.06}$ km s^{-1} pc^{-1}, and an expansion age of 10 ± 2 Myr would have $\kappa = 0.10 \pm 0.02$ km s^{-1} pc^{-1}. Given that we are only able to obtain a lower limit on the expansion age for US and our expansion data are statistically consistent with no expansion, we do not consider our 99% confidence lower limit in the final age determination for US.

[11] Distances are simply the inverse of the trigonometric parallax.

Table 12
Properties of Upper Sco Members Used For Expansion Age

HIP	d (pc)	v_{rad}(pred.) (km s^{-1})	v_{rad}(obs.) (km s^{-1})	References
76071	175 ± 20	−5.3	−6.1 ± 2.3	1
76310	151 ± 13	−4.4	−2.5 ± 0.6	1
76503	190 ± 13	−4.4	3.7 ± 20.0	2
76633	145 ± 18	−6.2	−2.8 ± 2.2	3
77635	152 ± 6	−5.0	−3.0 ± 4.7	3
77813	105 ± 14	−6.8	−5.4 ± 0.4	4
77840	154 ± 12	−5.2	−9.3 ± 1.6	3
77858	129 ± 9	−5.4	−6.3 ± 20.0	2
77859	131 ± 6	−5.6	−9.2 ± 3.1	3
77900	158 ± 12	−4.6	−1.3 ± 2.6	3
77909	158 ± 11	−5.2	−8.7 ± 4.3	3
77911	148 ± 12	−5.9	−2.9 ± 2.6	1
78099	141 ± 15	−5.9	−6.5 ± 2.9	3
78104	145 ± 4	−4.2	3.3 ± 20.0	2
78207	143 ± 5	−8.3	1.5 ± 2.2	1
78246	170 ± 7	−5.5	−12.1 ± 3.4	3
78265	180 ± 21	−5.1	−11.7 ± 10.0	2
78530	157 ± 13	−6.4	−9.0 ± 4.4	3
78549	146 ± 12	−6.2	−5.0 ± 5.0	3
78663	144 ± 24	−4.1	−11.3 ± 0.3	4
78809	144 ± 12	−6.0	−5.5 ± 3.2	1
78820	124 ± 12	−7.1	−1.0 ± 2.0	3
78847	162 ± 21	−6.5	−23.0 ± 3.0	1
78877	161 ± 17	−6.0	−6.6 ± 4.3	3
78933	145 ± 5	−6.9	−4.4 ± 3.0	3
78996	108 ± 10	−6.0	−7.9 ± 2.0	1
79031	119 ± 6	−5.9	−4.9 ± 2.8	3
79054	139 ± 20	−6.0	−4.1 ± 0.7	4
79098	136 ± 6	−6.1	−16.0 ± 5.4	5
79124	123 ± 10	−7.4	−18.1 ± 1.9	1
79156	170 ± 26	−7.3	−3.7 ± 1.9	1
79252	126 ± 35	−6.6	−3.8 ± 0.3	4
79258	114 ± 14	−3.6	−18.0 ± 0.3	4
79288	150 ± 22	−5.7	−2.9 ± 0.3	4
79369	122 ± 21	−6.9	−6.7 ± 0.3	4
79374	145 ± 16	−7.4	−14.2 ± 1.6	5
79404	147 ± 3	−5.0	−3.8 ± 10.0	2
79410	140 ± 22	−7.3	−6.2 ± 2.6	1
79439	132 ± 19	−7.4	−5.6 ± 0.2	1
79530	144 ± 13	−6.0	3.4 ± 2.5	3
79596	175 ± 11	−3.6	−22.6 ± 0.4	3
79599	109 ± 7	−7.0	−7.8 ± 1.7	3
79622	149 ± 9	−5.8	−8.4 ± 2.7	3
79785	101 ± 6	−7.0	−6.4 ± 0.2	1
79878	129 ± 8	−5.1	−3.4 ± 0.6	1
79910	149 ± 33	−7.0	−6.6 ± 0.7	4
79977	123 ± 16	−7.1	−2.8 ± 0.3	4
80019	173 ± 33	−7.4	−15.0 ± 3.9	5
80024	163 ± 21	−7.4	−4.0 ± 1.4	1
80088	139 ± 34	−6.8	−7.5 ± 2.2	1
80126	151 ± 13	−6.5	−3.0 ± 6.5	5
80320	142 ± 23	−4.8	1.7 ± 0.3	4
80324	110 ± 12	−3.8	−2.1 ± 1.5	3
80461	125 ± 12	−6.6	−6.8 ± 2.9	5
80473	111 ± 11	−6.6	−11.4 ± 3.0	3
80474	135 ± 11	−6.7	−11.0 ± 2.4	5
80493	135 ± 16	−5.8	−7.4 ± 1.9	1
80535	120 ± 17	−5.5	−4.0 ± 0.3	4
80569	161 ± 6	−8.1	−19.0 ± 2.1	3
80763	170 ± 29	−5.9	−3.5 ± 0.8	3
80896	142 ± 25	−4.9	3.3 ± 2.7	1
81266	145 ± 11	−5.5	1.7 ± 0.9	3
81455	105 ± 15	−5.2	−3.2 ± 0.5	4
82218	136 ± 20	−8.2	−6.7 ± 0.3	4
82319	104 ± 19	−7.4	−18.3 ± 1.3	1

Notes. Distances are derived using trigonometric parallaxes from van Leeuwen (2007).
References. (1) Dahm et al. 2011; (2) Duflot et al. 1995; (3) Gontcharov 2006; (4) Chen et al. 2011; (5) Barbier-Brossat & Figon 2000.

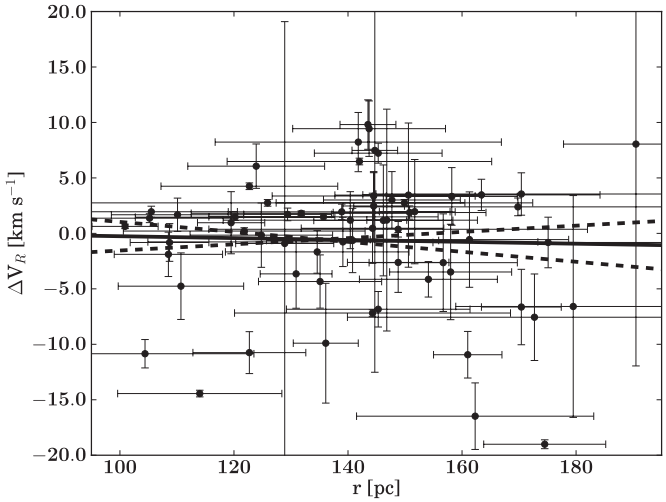

Figure 16. Distance (r) vs. the difference between the observed and predicted radial velocity (V_R). The sample includes US candidate members from de Zeeuw et al. (1999) within 50 pc of the mean US distance and with measured radial velocities within 20 km s^{-1} of the predicted value. If US is expanding, the closest members should be more blueshifted and the further members should be more redshifted. A series of Monte Carlo simulations gives a best-fit slope of $\kappa = -0.01 \pm 0.04$ km s^{-1} pc^{-1}, which places a 99% confidence lower limit on the expansion age of 10.5 Myr.

Table 13
Upper Sco Age Estimates

Sample	Age (Myr)
F-Type PMS	13 ± 1
Main-sequence Turnoff	10 ± 2
Antares	12 ± 2
A-Type Turn-on	10 ± 3
G-Type PMS	9 ± 2
Adopted Age	11
Statistical uncertainty	±1
Systematic uncertainty	±2

5.7. What is the Best Median Age for Upper Sco?

Every age indicator we have examined thus far has yielded an age of Upper Sco of 9–13 Myr, summarized in Table 13. The youngest median age comes from the G-type stars at ∼9 Myr, and the oldest from the F-type stars at ∼13 Myr, so we can conclude with confidence that US must be between 9 and 13 Myr old. Regarding each segment of the H-R diagram as independent, we simply take the mean age of our values—∼10 Myr for the main-sequence turnoff, ∼12 Myr for Antares, ∼10 Myr for the A-type stars, ∼13 Myr for the F-type members, and ∼9 Myr for the G-type members. This gives a final adopted age of 11 ± 1 Myr (s.e.m., statistical) for Upper Sco, which is more than twice the currently accepted age (Preibisch et al. 2002). As each segment of the H-R diagram provides an independent age, we estimate our systematic uncertainty as the 1σ dispersion of these independent ages, which yields a systematic uncertainty of ±2 Myr.

5.8. Implications of an Older Upper Sco

Upper Sco has been a benchmark stellar population in studies of circumstellar disk lifetimes (e.g., Carpenter et al. 2006), but has a lower primordial disk fraction when compared to other stellar populations at 5 Myr (e.g., λ Ori; Barrado y Navascués

et al. 2007). Considered in the context of 11 Myr age, the observed primordial disk fraction is consistent with those of similarly aged stellar populations (e.g., NGC 7160; Sicilia-Aguilar et al. 2006). Our detailed analysis of the isochronal ages for massive and intermediate-mass Upper Sco stars may indicate that the ages of similarly aged groups may also be due for further investigation and significant revision. Naylor (2009) has also found evidence that the nuclear ages for massive stars in <10 Myr old groups are typically 1.5–2× the pre-MS contraction ages. In particular, Naylor (2009) finds that two of Upper Sco's ∼5 Myr old siblings (NGC 2362 and Cep OB3b, each with pre-MS ages of 4.5 Myr) have best-fit isochronal ages for the massive stars of 9.1 Myr and 10 Myr, respectively. In this regard the doubling of Upper Sco's age does not seem surprising. Naylor (2009) has proposed that the nuclear ages may be the more correct ones, and that protoplanetary disks may correspondingly have nearly twice as long to form gas giant planets as previously believed.

In addition to circumstellar disk studies, Upper Sco has been the subject of many surveys for low-mass companions (e.g., Lafrenière et al. 2008; Ireland et al. 2011). A low-mass companion to [PZ99] J160930.3-210459[12] was discovered at a very large separation by Lafrenière et al. (2008). The mass[13] of this companion was determined to be 8 $M_{\rm Jup}$ using the assumed age of 5 Myr. However, we use our revised age for Upper Sco of 11 Myr and the object's reported $T_{\rm eff}$ of 1800 ± 200 K (Lafrenière et al. 2010) to obtain a mass of 13^{+2}_{-3} $M_{\rm Jup}$ using the DUSTY models (Chabrier et al. 2000; Baraffe et al. 2002). Alternatively, using the object's bolometric luminosity of $\log(L/L_{\odot}) = -3.55 \pm 0.2$ (Lafrenière et al. 2010) and the 11 Myr age we estimate a mass of 14^{+2}_{-3} $M_{\rm Jup}$, consistent with the estimates from $T_{\rm eff}$. Here we follow Lafrenière et al. (2010) and adopt the estimates from the luminosity, listed in Table 14. Similarly, a companion to GSC 06214-00210 was discovered by Ireland et al. (2011) and thought to have a mass of ∼14 $M_{\rm Jup}$ at an age of 5 Myr. However, at an age of 11 Myr the mass is slightly higher at 17 ± 3 $M_{\rm Jup}$, using the DUSTY models and the estimated absolute magnitudes $M_J \sim 10.5$, $M_H \sim 9.6$, $M_K \sim 9.1$ (Ireland et al. 2011). The substellar companion to HIP 78530 (Lafrenière et al. 2011) was estimated to have a mass of ∼21–26 $M_{\rm Jup}$ with an assumed age of 5 ± 1 Myr. We use the bolometric luminosity of $\log(L/L_{\odot}) = -2.55 \pm 0.13$ (Lafrenière et al. 2011) and our revised age of 11 Myr to obtain a mass for HIP 78530B of 30^{+17}_{-8} $M_{\rm Jup}$. The substellar companion to the young brown dwarf UScoCTIO 108 has a mass of 14^{+2}_{-8} $M_{\rm Jup}$ with an assumed age of 5–6 Myr (Béjar et al. 2008). Using the reported luminosity of $\log(L/L_{\odot}) = -3.14 \pm 0.20$ (Béjar et al. 2008) and our revised age of 11 Myr, we estimate a mass of 16 ± 2 $M_{\rm Jup}$ for UScoCTIO 108b. The substellar binary Oph J1622-2405 initially had component mass estimates of ∼14 $M_{\rm Jup}$ and ∼7 $M_{\rm Jup}$ based on an assumed age of 1 Myr (Jayawardhana & Ivanov 2006). However, follow-up spectroscopic studies (Allers et al. 2007; Close et al. 2007; Luhman et al. 2007) found higher masses. Here we estimate the masses using the effective temperatures from Luhman et al. (2007) with our revised age of 11 Myr and find masses of 53^{+9}_{-7} $M_{\rm Jup}$ and 21 ± 3 $M_{\rm Jup}$ for Oph J1622-2405A and Oph J1622-2405B, respectively, with the DUSTY models. This is in agreement with the results from Luhman et al. (2007), who used H-R diagram positions with the DUSTY models for their mass estimates. The revised mass estimates discussed above are summarized in Table 14. Hence, we believe that none of the substellar companions directly imaged in Upper Sco have inferred masses below the deuterium-burning limit.

Table 14
Revised Mass Estimates for Substellar Objects in Upper Sco

Object	Mass at 11 Myr ($M_{\rm Jup}$)
[PZ99] J160930.3-210459b	14^{+2}_{-3}
GSC 06214-00210b	17 ± 3
HIP 78530B	30^{+17}_{-8}
UScoCTIO 108B	16^{+3}_{-2}
Oph 1622-2405A	53^{+9}_{-7}
Oph 1622-2405B	21 ± 3

Notes. Masses estimated using the DUSTY models of Chabrier et al. (2000) and Baraffe et al. (2002) and an age for Upper Sco of 11 ± 2 Myr.

Sco-Cen has been used as an example of triggered star formation, with supernova in UCL/LCC triggering star formation in US and supernova in US triggering star formation in ρ Oph (de Geus 1992; Preibisch & Zinnecker 1999). The UCL shell has an expansion velocity of 10 ± 2 km s^{-1} and radius 110 ± 10 pc, suggesting it originated in UCL ∼ 11 Myr ago and passed through US about 4 Myr ago (de Geus 1992). However, given the revised age estimates for US, it does not seem likely that the passage of this superbubble would have triggered star formation in US since it would have arrived too late. However, this does not mean that star formation in US was not triggered by UCL, it simply means that the timescales and ages are not consistent with the arrival of the UCL shell in US as the triggering event. Similarly, the shell around US has an expansion velocity of 10 ± 2 km s^{-1} and a radius of 40 ± 4 pc, consistent with an age for the shell of ∼4 Myr. At 10 km s^{-1} it would have traveled the ∼15 pc from US to ρ Oph in about 1.5 Myr. With the revised 11 Myr age for US and ρ Oph ages of ∼2–3 Myr (Erickson et al. 2011), there is sufficient time for star formation in ρ Oph to have been triggered by the US shell.

Another important implication of our result is to drive down the inferred progenitor mass for the runaway young neutron star RX J1856.5-3754. Tetzlaff et al. (2011) claim that RX J1856 formed in Upper Sco and was ejected 0.5 Myr ago. Assuming a

[12] Although the star is commonly called 1RXS J160929.1-210524 or 1RXS 1609, this is technically not an appropriate name. 1RXS is one of the acronyms used for *ROSAT* X-ray sources, however it refers to the X-ray source itself rather than any optical counterpart, as sometimes there may be multiple plausible optical counterparts (hence why one does not normally encounter stars called by 1RXS names in the literature, but by "RX J" names or others). The likely optical counterpart (star) was first identified as a pre-MS Upper Sco member in Preibisch et al. (1998) (listed as GSC 6213-1358) and later was referred to as "Upper Sco 160930.3-210459" in Preibisch & Zinnecker (1999). SIMBAD standardized the "Upper Sco" names to "[PZ99] J" to comply with IAU guidelines for position-based names, and the [PZ99] J-names are now in common use.

[13] This companion was considered the first directly imaged exoplanet orbiting a Sun-like star. The discoverers considered the companion a "planet" (Lafrenière et al. 2010) based on their calculated mass and demonstration of common motion, following the IAU Working Group on Extrasolar Planets (WGESPs) definition, which defined a planet as "objects with true masses below the limiting mass for thermonuclear fusion of deuterium (currently calculated to be 13 Jupiter masses for objects of solar metallicity) that orbit stars or stellar remnants"; see http://www.dtm.ciw.edu/boss/definition.html and Boss et al. (2007). Recent work by Spiegel et al. (2011) shows that objects with protosolar composition and masses of >11.9 $M_{\rm Jup}$ can burn at least 10% of their initial deuterium over 10 Gyr. Hence, following the definition of "planet" and "brown dwarf" adopted by the IAU and the discoverers, the companion should probably be best considered a "brown dwarf." Given that the GSC or [PZ99] designation should be preferred over the 1RXS name, the brown dwarf companion should probably be called "GSC 06213-01358 B" or "[PZ99] J160930.3-210459 B."

progenitor age of 5 Myr, Tetzlaff et al. (2011) predicted that the progenitor would have had a mass of ∼37–45 $M_{\odot}$ and main-sequence spectral type of O5-O7. Smartt (2009) reviewed the observational and theoretical constraints on the supernovae and their progenitors, and suggests that progenitors with masses of >30 $M_{\odot}$ almost certainly form black holes, not neutron stars. However, if the progenitor of J1856 was a 10.5 Myr old star when it exploded 0.5 Myr ago, then the progenitor was most likely a ∼18–20 $M_{\odot}$ O9-type star (using the Ekström et al. 2011 tracks), with the remnant being either a neutron star or black hole (likely depending on the rotation or whether it was in an interacting binary; Smartt 2009). Indeed, if the empirically constrained set of supernova outcomes outlined by Smartt (2009) are correct, and if one adopts the previous age of 5 Myr, then the deceased high-mass stars in Upper Sco should have *all* turned into black holes. This would leave the "young" neutron star RX J1856 with a well-constrained distance and proper motion but without a plausible birth site. We conclude that the RX J1856 runaway scenario is more plausible if Upper Sco is 11 Myr old, and the progenitor would have been a much easier to form ∼18–20 $M_{\odot}$ star rather than a rarer ∼37–45 $M_{\odot}$ star.

6. CONCLUSIONS

We can summarize our conclusions as follows.

1. The PMS "turn-on" for UCL and LCC occurs near spectral type ∼F2 and ∼F4, respectively. The F-type members of US appear to be all PMS. Examining the A-type members of US allows us to estimate the PMS turn-on for US to be near spectral type ∼A3.
2. The good agreement between the isochronal ages of F-type stars studied here and the G- and K-type stars studied in Mamajek et al. (2002) provides greater confidence in those ages, and more firmly establishes that UCL is slightly younger than, or roughly coeval with, LCC. In order of youngest to oldest: US, UCL, LCC.
3. The median ages obtained with the PMS F-type members (those later than F5) for UCL and LCC agree with previous results for early-B-type stars and PMS G-type stars (Mamajek et al. 2002), with median ages of 16 ± 1 Myr and 17 ± 1 Myr, respectively.
4. The F-type members have a median isochronal age of 13 ± 1 Myr (68% CL) for US, which is much older than previous results. Using the approximate PMS turn-on point with the A-type stars allows us to estimate an age of 10 ± 3 Myr. Re-examining the early-B-type stars and the G-type PMS stars in US yields median ages of 10 ± 2 Myr and 9 ± 2 Myr, respectively. Age estimates for the M1.5Iab-Ib supergiant US member Antares give 12^{+3}_{-1} Myr. Considering these to be independent estimates, we obtain an overall mean age for Upper Sco of 11 ± 1 ± 2 Myr (statistical, systematic) with the uncertainty in the mean age dominated by systematic differences between the isochronal ages inferred from different mass ranges.
5. We find a 99% confidence lower limit on the kinematic expansion age for Upper Sco of 10.5 Myr using trigonometric parallax and radial velocity data. However, the astrometry and radial velocities are statistically consistent with no expansion.
6. Based on Hα emission accretion diagnostics, we estimate a spectroscopic accretion disk fraction of 0/17 (<19%; 95% CL) in US, consistent with the *Spitzer* results of Carpenter et al. (2006) of 0/30 (<11%; 95% CL) for F- and G-type stars. In UCL we find 1/41 (2^{+5}_{-1}%; 68% CL) accretors and in LCC we find 1/50 (2^{+4}_{-1}%; 68% CL) accretors, which are both consistent with the spectroscopic accretion disk fraction for the G- and K-type members of UCL and LCC from Mamajek et al. (2002) for G- and K-type stars.
7. The revised age of 11 Myr for Upper Sco may explain the lower than expected disk fraction compared to 5 Myr groups (e.g., λ Ori; Barrado y Navascués et al. 2007). We reevaluate the masses of the known substellar companions in Upper Sco using available published data and our revised age of 11 Myr and find that inferred masses are typically ∼20%–70% more massive than previously estimated. All of the imaged companions thus far appear to be more massive than the deuterium-burning limit and so none of the companions are in the planetary-mass regime. In addition to larger substellar masses, the older age for Upper Sco implies a more realistic, lower progenitor mass of ∼18–20 $M_{\odot}$ for the young neutron star RX J1856.5-3754.

We thank Fred Walter for the use of his SMARTS RC-spectrograph pipeline for reducing the data obtained at the SMARTS 1.5 m telescope at Cerro Tololo, Chile, as well as Jose Velasquez and Manuel Hernandez for their help and advice at the telescope. University of Rochester is a member of the Small and Moderate Aperture Research Telescope System (SMARTS) Consortium. This work has been supported by NSF grant AST-1008908 and funds from the School of Arts and Sciences at the University of Rochester.

Note added in proof. In Section 5.1, we should include an additional age estimate for Upper Sco of 8–10 Myr by Sartori et al. (2003), who also found an older age for Upper Sco.

REFERENCES

Abt, H. A. 1981, ApJS, 45, 437
Abt, H. A. 1986, PASP, 98, 307
Abt, H. A., & Morrell, N. I. 1995, ApJS, 99, 135
Alencar, S. H. P., Melo, C. H. F., Dullemond, C. P., et al. 2003, A&A, 409, 1037
Allers, K. N., Jaffe, D. T., Luhman, K. L., et al. 2007, ApJ, 657, 511
Andersen, J., Lindgren, H., Hazen, M. L., & Mayor, M. 1989, A&A, 219, 142
Balachandran, S. 1991, Mem. Soc. Astron. Ital., 62, 33
Balona, L. A. 1994, MNRAS, 268, 119
Baraffe, I., Chabrier, G., Allard, F., & Hauschildt, P. H. 2002, A&A, 382, 563
Barbier-Brossat, M., & Figon, P. 2000, A&AS, 142, 217
Barrado y Navascués, D., Stauffer, J. R., Morales-Calderón, M., et al. 2007, ApJ, 664, 481
Béjar, V. J. S., Zapatero Osorio, M. R., Pérez-Garrido, A., et al. 2008, ApJ, 673, L185
Bertelli, G., Bressan, A., Chiosi, C., Fagotto, F., & Nasi, E. 1994, A&AS, 106, 275
Bertone, E., Buzzoni, A., Chávez, M., & Rodríguez-Merino, L. H. 2004, AJ, 128, 829
Bessell, M. S., Castelli, F., & Plez, B. 1998, A&A, 333, 231
Bevington, P. R., & Robinson, D. K. (ed.) 2003, Data Reduction and Error Analysis for the Physical Sciences (3rd ed.; New York: McGraw-Hill)
Bidelman, W. P. 1956, PASP, 68, 318
Bitner, M. A., Chen, C. H., Muzerolle, J., et al. 2010, ApJ, 714, 1542
Blaauw, A. 1956, ApJ, 123, 408
Blaauw, A. 1964, in IAU Symp. 20, The Galaxy and the Magellanic Clouds, ed. F. J. Kerr (Cambridge: Cambridge Univ. Press), 50
Blaauw, A. 1978, in Problems of Physics and Evolution of the Universe, ed. L. V. Mirzoyan (Yerevan: Publishing House of the Armenian Academy of Sciences), 101
Boss, A. P., Butler, R. P., Hubbard, W. B., et al. 2007, in IAU Transactions 26A, Reports on Astronomy 2002–2005, ed. O. Engvold (Cambridge: Cambridge University Press), 183

Briceño, C., Preibisch, T., Sherry, W. H., et al. 2007, in Protostars and Planets V, ed. B. Reipurth, D. Jewitt, & K. Keil (Tucson, AZ: Univ. Arizona Press), 345
Brown, A. G. A., Dekker, G., & de Zeeuw, P. T. 1997, MNRAS, 285, 479
Brown, A. G. A., & Verschueren, W. 1997, A&A, 319, 811
Carpenter, J. M., Mamajek, E. E., Hillenbrand, L. A., & Meyer, M. R. 2006, ApJ, 651, L49
Casagrande, L., Flynn, C., & Bessell, M. 2008, MNRAS, 389, 585
Casagrande, L., Portinari, L., & Flynn, C. 2006, MNRAS, 373, 13
Casagrande, L., Ramírez, I., Meléndez, J., Bessell, M., & Asplund, M. 2010, A&A, 512, A54
Chabrier, G., Baraffe, I., Allard, F., & Hauschildt, P. 2000, ApJ, 542, 464
Chen, C. H., Mamajek, E. E., Bitner, M. A., et al. 2011, ApJ, 738, 122
Claret, A. 2004, A&A, 424, 919
Close, L. M., Zuckerman, B., Song, I., et al. 2007, ApJ, 660, 1492
Code, A. D., Bless, R. C., Davis, J., & Brown, R. H. 1976, ApJ, 203, 417
Conti, P. S., Leep, E. M., & Lorre, J. J. 1977, ApJ, 214, 759
Cowley, A., Cowley, C., Jaschek, M., & Jaschek, C. 1969, AJ, 74, 375
Dahm, S. E., Slesnick, C. L., & White, R. J. 2011, arXiv:1110.0536
D'Antona, F., & Mazzitelli, I. 1997, Mem. Soc. Astron. Ital., 68, 807
de Bruijne, J. H. J. 1999a, MNRAS, 306, 381
de Bruijne, J. H. J. 1999b, MNRAS, 310, 585
de Bruijne, J. H. J., Hoogerwerf, R., & de Zeeuw, P. T. 2001, A&A, 367, 111
de Geus, E. J. 1992, A&A, 262, 258
de Geus, E. J., de Zeeuw, P. T., & Lub, J. 1989, A&A, 216, 44
de Zeeuw, P. T., Hoogerwerf, R., de Bruijne, J. H. J., Brown, A. G. A., & Blaauw, A. 1999, AJ, 117, 354
de Zeeuw, T., & Brand, J. 1985, in ASSL vol. 120, Birth and Evolution of Massive Stars and Stellar Groups, ed. W. Boland & H. van Woerden (Dordrecht: Reidel), 9
Demarque, P., Woo, J.-H., Kim, Y.-C., & Yi, S. K. 2004, ApJS, 155, 667
Dotter, A., Chaboyer, B., Jevremović, D., et al. 2008, ApJS, 178, 89
Duflot, M., Figon, P., & Meyssonnier, N. 1995, A&AS, 114, 269
Ekström, S., Georgy, C., Eggenberger, P., et al. 2011, arXiv:1110.5049
Elliot, J. L., Rages, K., & Veverka, J. 1976, ApJ, 207, 994
Erickson, K. L., Wilking, B. A., Meyer, M. R., Robinson, J. G., & Stephenson, L. N. 2011, AJ, 142, 140
Fiorucci, M., & Munari, U. 2003, A&A, 401, 781
Flower, P. J. 1996, ApJ, 469, 355
Garmany, C. D., Conti, P. S., & Massey, P. 1980, ApJ, 242, 1063
Garrison, R. F. 1967, ApJ, 147, 1003
Glaspey, J. W. 1971, PhD thesis, Univ. Arizona
Glaspey, J. W. 1972, AJ, 77, 474
Gontcharov, G. A. 2006, Astron. Lett., 32, 759
Gott, J. R., III, Vogeley, M. S., Podariu, S., & Ratra, B. 2001, ApJ, 549, 1
Gray, R. O. 1989, AJ, 98, 1049
Gray, R. O., & Corbally, C. J. 1998, AJ, 116, 2530
Gray, R. O., & Corbally, C. J. 2002, AJ, 124, 989
Gray, R. O., & Corbally, C. J. 2009, Stellar Spectral Classification (Princeton, NJ: Princeton Univ. Press)
Gray, R. O., Corbally, C. J., Garrison, R. F., et al. 2006, AJ, 132, 161
Gray, R. O., & Garrison, R. F. 1989, ApJS, 69, 301
Gray, R. O., Napier, M. G., & Winkler, L. I. 2001, AJ, 121, 2148
Hauck, B., & Mermilliod, M. 1998, A&AS, 129, 431
Hernández, J., Calvet, N., Hartmann, L., et al. 2005, AJ, 129, 856
Herrero, A., Kudritzki, R. P., Vilchez, J. M., et al. 1992, A&A, 261, 209
Høg, E., Fabricius, C., Makarov, V. V., et al. 2000, A&A, 355, L27
Hoogerwerf, R., & Aguilar, L. A. 1999, MNRAS, 306, 394
Hoogerwerf, R., de Bruijne, J. H. J., & de Zeeuw, P. T. 2000, ApJ, 544, L133
Houk, N. 1978, Michigan Catalogue of Two-dimensional Spectral Types for the HD Stars (Ann Arbor, MI: Dept. of Astronomy, Univ. of Michigan: distributed by University Microfilms International)
Houk, N. (ed.) 1982, in Michigan Spectral Survey (Ann Arbor, MI: Dept. of Astronomy, Univ. of Michigan), 3
Houk, N., & Cowley, A. P. (ed.) 1975, University of Michigan Catalogue of Two-dimensional Spectral Types for the HD Stars (Ann Arbor, MI: Dept. of Astronomy, Univ. of Michigan)
Houk, N., & Smith-Moore, M. (ed.) 1988, in Michigan Spectral Survey, Vol. 4 (Ann Arbor, MI: Dept. of Astronomy, Univ. of Michigan)
Iben, I., Jr. 1965, ApJ, 141, 993
Ireland, M. J., Kraus, A., Martinache, F., Law, N., & Hillenbrand, L. A. 2011, ApJ, 726, 113
Jayawardhana, R., & Ivanov, V. D. 2006, Science, 313, 1279
Johnson, H. L., & Morgan, W. W. 1953, ApJ, 117, 313
Keenan, P. C., & McNeil, R. C. 1989, ApJS, 71, 245
Lada, C. J., & Lada, E. A. 2003, ARA&A, 41, 57
Lafrenière, D., Jayawardhana, R., Janson, M., et al. 2011, ApJ, 730, 42
Lafrenière, D., Jayawardhana, R., & van Kerkwijk, M. H. 2008, ApJ, 689, L153
Lafrenière, D., Jayawardhana, R., & van Kerkwijk, M. H. 2010, ApJ, 719, 497
Levesque, E. M., Massey, P., Olsen, K. A. G., et al. 2005, ApJ, 628, 973
Luhman, K. L., Allers, K. N., Jaffe, D. T., et al. 2007, ApJ, 659, 1629
Maeder, A. 1981, A&A, 102, 401
Maeder, A., & Meynet, G. 2000, ARA&A, 38, 143
Mamajek, E. E. 2005, ApJ, 634, 1385
Mamajek, E. E. 2009, in AIP Conf. Ser. 1158, Exoplanets and Disks: Their Formation and Diversity, ed. T. Usuda, M. Tamura, & M. Ishii (Melville, NY: AIP), 3
Mamajek, E. E., Meyer, M. R., & Liebert, J. 2002, AJ, 124, 1670
Mamajek, E. E., Meyer, M. R., & Liebert, J. 2006, AJ, 131, 2360
Mermilliod, J. C. 2006, VizieR Online Data Catalog, 2168, 0
Meyer, M. R., Calvet, N., & Hillenbrand, L. A. 1997, AJ, 114, 288
Meynet, G., & Maeder, A. 2000, A&A, 361, 101
Mora, A., Merín, B., Solano, E., et al. 2001, A&A, 378, 116
Morgan, W. W., & Abt, H. A. 1973, AJ, 78, 386
Morgan, W. W., Abt, H. A., & Tapscott, J. W. 1978, Revised MK Spectral Atlas for Stars Earlier Than the Sun (Williams Bay: Yerkes Obs.; Tucson: KPNO)
Morgan, W. W., & Hiltner, W. A. 1965, ApJ, 141, 177
Morgan, W. W., & Keenan, P. C. 1973, ARA&A, 11, 29
Naylor, T. 2009, MNRAS, 399, 432
Neckel, T., & Klare, G. 1980, A&AS, 42, 251
North, J. R., Davis, J., Tuthill, P. G., Tango, W. J., & Robertson, J. G. 2007, MNRAS, 380, 1276
Paunzen, E., Duffee, B., Heiter, U., Kuschnig, R., & Weiss, W. W. 2001, A&A, 373, 625
Perryman, M. A. C. ESA. (ed.) 1997, The HIPPARCOS and TYCHO Catalogues (ESA Special Publication, Vol. 1200; Noordwijk: ESA Publications Division)
Preibisch, T., Brown, A. G. A., Bridges, T., Guenther, E., & Zinnecker, H. 2002, AJ, 124, 404
Preibisch, T., Guenther, E., Zinnecker, H., et al. 1998, A&A, 333, 619
Preibisch, T., & Mamajek, E. 2008, in Handbook of Star Forming Regions, Volume II: The Southern Sky, Vol. 5, ed. B. Reipurth (San Francisco, CA: ASP), 235
Preibisch, T., & Zinnecker, H. 1999, AJ, 117, 2381
Reid, A. H. N., Bolton, C. T., Crowe, R. A., et al. 1993, ApJ, 417, 320
Richichi, A., & Lisi, F. 1990, A&A, 230, 355
Sartori, M. J., Lepine, J. R. D., & Dias, W. S. 2003, A&A, 404, 913
Shobbrook, R. R. 1983, MNRAS, 205, 1215
Sicilia-Aguilar, A., Hartmann, L., Calvet, N., et al. 2006, ApJ, 638, 897
Siess, L., Dufour, E., & Forestini, M. 2000, A&A, 358, 593
Skrutskie, M. F., Cutri, R. M., Stiening, R., et al. 2006, AJ, 131, 1163
Slesnick, C. L., Hillenbrand, L. A., & Carpenter, J. M. 2008, ApJ, 688, 377
Smartt, S. J. 2009, ARA&A, 47, 63
Spiegel, D. S., Burrows, A., & Milsom, J. A. 2011, ApJ, 727, 57
Stauffer, J., Tanner, A. M., Bryden, G., et al. 2010, PASP, 122, 885
Stickland, D. J., Lloyd, C., Koch, R. H., & Pachoulakis, I. 1996, Observatory, 116, 387
Talon, S., Zahn, J.-P., Maeder, A., & Meynet, G. 1997, A&A, 322, 209
Tango, W. J., Davis, J., Jacob, A. P., et al. 2009, MNRAS, 396, 842
Tetzlaff, N., Eisenbeiss, T., Neuhäuser, R., & Hohle, M. M. 2011, MNRAS, 417, 617
Torres, C. A. O., Quast, G. R., da Silva, L., et al. 2006, A&A, 460, 695
Valdes, F., Gupta, R., Rose, J. A., Singh, H. P., & Bell, D. J. 2004, ApJS, 152, 251
van Leeuwen, F. 2007, A&A, 474, 653
Vieira, S. L. A., Corradi, W. J. B., Alencar, S. H. P., et al. 2003, AJ, 126, 2971
White, R. J., & Basri, G. 2003, ApJ, 582, 1109
Wright, J. T. 2005, AJ, 129, 1776